Communications Research Centre

MEASUREMENTS AND MODELLING OF THE HF RADIO NOISE ENVIRONMENT NEAR AN HVDC CONVERTER STATION

by

W.R. LAUBER AND J.M. BERTRAND

Ministère des Communications

CRC REPORT NO. 1362

OTTAWA, MARCH 1983

COMMUNICATIONS RESEARCH CENTRE

DEPARTMENT OF COMMUNICATIONS
CANADA

MEASUREMENTS AND MODELLING OF THE HF RADIO NOISE ENVIRONMENT NEAR AN HVDC CONVERTER STATION

by

W.R. Lauber and J.M. Bertrand

(Radar and Communications Technology Branch)

CRC REPORT NO. 1362

March 1983

OTTAWA

TABLE OF CONTENTS

MEASUREMENTS AND MODELLING OF THE HF RADIO NOISE ENVIRONMENT NEAR AN HVDC CONVERTER STATION

by

W.R. Lauber and J.M. Bertrand

ABSTRACT

Measurements of the HF radio noise environment near an HVDC transmission line and converter station were made outside Winnipeg in July 1977. Typical levels and characteristics are presented for various combinations of mercury arc valve noise, AC hum and DC corona from a number of sites within eight kilometres of the converter station. In addition, two sets of measurements were taken 80 km from the converter station. Values of the root-mean-square, average and quasipeak voltages were calculated from the Amplitude Probability Distributions (APDs) of the noise and were found to compare favourably with the directly measured values. Four mathematical models, the Rayleigh and three others which were developed for atmospheric noise were fitted to the measured APD data. Using inputs of V_{rms} and V_d the Log-Normal model produced the most accurate predictions of the measured APDs. The Log-Normal and the Hall models both fitted the measured Average Crossing Rate data equally well.

1. INTRODUCTION

1.1 BACKGROUND

The major sources of man-made radio noise are being studied as part of an ongoing program at the Communications Research Centre (CRC) to measure and characterize the radio noise environment. This radio noise environment

must be characterized before one either tries to reduce the levels or to improve the communication system operating in it. The underlying aim of this work is to study the effects of the radio noise environment on communication systems with the study of the physics of the noise generation process being left to other workers; e.g., those in the power industry or automotive industry.

In October, 1974, statistical measurements were made of AC powerline noise at the Apple Grove 775 kV project as part of the IEEE Power Engineering Society's field comparison of RI and TVI instrumentation [1, 2]. The statistical parameters measured on this test were: V_{rms}, V_d (Voltage deviation) and Amplitude Probability Distribution (APD). The results from this brief test were encouraging, thus, as a follow-up, it was decided to obtain a large sample of statistical data.

In Central Canada, there is an 895 km long HVDC (High Voltage Direct Current) powerline capable of operating at ± 450 kV that runs from the Nelson River on Hudson's Bay to Winnipeg (see map in Figure 1). Because of low water conditions in the north in late spring 1977, this operating line was shut down for periods of six hours a day. During this down time, measurements could be made to simulate the preconstruction radio noise environment around the line. During the measurements, the line was operated at a number of voltage conditions other than ± 450 kV depending on the load. Also, the converter valves (mercury-arc type) which convert the HVDC to AC for distribution were known to be a good source of impulsive radio noise. These valves are housed at Dorsey Converter Station which is located about 50 km North West of Winnipeg. For the above reasons, it was decided that this was an ideal line on which to obtain a large sample of statistical radio noise data. In addition to this work researchers at the National Research Council of Canada have also made basic radio noise and corona power loss measurements of this powerline [3, 4, 5].

1.2 OBJECTIVES

The objectives of these tests were:

(1) To make statistical measurements to characterize the radio noise environment near the HVDC powerline and converter station under various line operating conditions.

(2) To study the accuracy of computing V_{rms}, V_d, and V_{qp} (quasi peak) from APD data.

(3) To study the suitability of applying widely used mathematical models developed for atmospheric noise to man-made radio noise.

(4) To investigate the possibility of relating the statistical measurements to the physical characteristics of man-made radio noise.

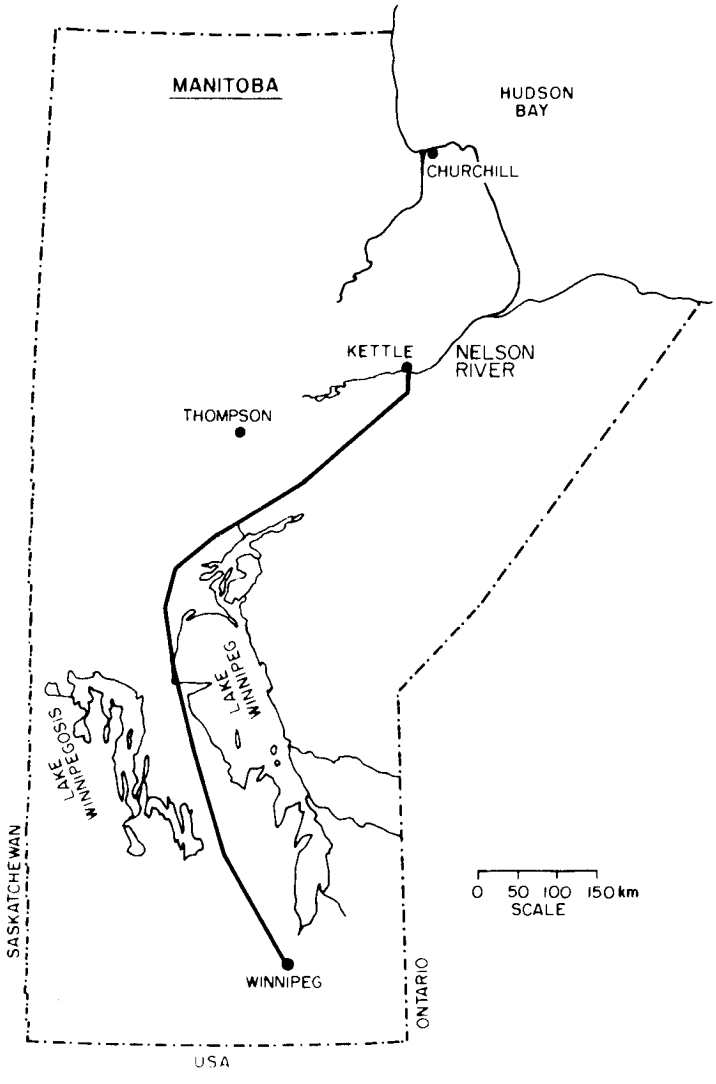

Figure 1. Map Showing Manitoba Hydro's HVDC Powerline

2. SCOPE

2.1 NOISE PARAMETERS

In any radio noise study, one would like to take the measurements that give as much useful data as possible. However, to suggest that it would be wrong to make simple measurements, e.g., V_{rms} or $V_{average}$, when it is now technically possible to measure statistical distributions would be incorrect. One must evaluate each case on the basis of the cost of making and using the more detailed measurements versus the benefits of more complete noise data. The measurements, however, must relate to the performance of the communication system using that part of the radio spectrum. Since modern communication systems use a wide variety of equipments and modulation techniques, the parameters used to determine the degree of degradation by a particular noise source must be statistical in nature. Finally, the measurements must be taken in such a way that they may be compared easily with measurements taken elsewhere by others. The following measurements were taken in this study:

(1) V_{rms} which is the most basic single parameter in communication theory [6, 7, 8] and is necessary in all signal to noise calculations.

(2) V_d (voltage deviation) which is directly related to the shape of the APD for atmospheric noise [9].

(3) V_{qp} (quasi peak) which has been shown to be empirically related to the performance of AM broadcast reception [10].

(4) APD which is necessary for predicting the performance of digital communication systems [11, 12, 13].

and (5) ACR (Average Crossing Rate) characteristic which has been used in studies that develop mathematical models of radio noise [14, 15, 16, 17]. It is also possible to relate the ACR back to the physical process in terms of a pulse repetition rate if the noise process consists, in part, of a periodic component.

2.2 EQUIPMENT

The equipment that was used to make these measurements was housed in a station wagon. A 9 foot rod antenna was mounted with its associated coupler and ground plane on the roof of the vehicle. A Singer (now AILTECH) NM-26T electromagnetic noise meter was used to produce the V_{rms} and V_d data. A separate Singer NM-25T field intensity meter was used to produce the V_{qp} data. A spectrum analyzer was used in the zero sweep mode, tuned to 455 KHz to give a time display of the noise from the IF output of the NM-26T. When the NM-26T was operated in the Peak mode (fixed AGC) the IF output was used to drive the Radio Noise Analyzer (RNA) [18] that produced the APD and ACR data.

The RNA (see block diagram in Figure 2) uses an envelope detector on the 455 KHz IF output from the NM-26T and quantizes it into 15 discrete levels each spaced 6 dB apart. In the APD mode, the percentage of time that the IF envelope exceeds each quantizer level is computed. In the ACR mode, the number of times per second that the IF envelope crosses each quantizer level in the positive direction is computed. Since it is difficult to build a single stage detector with a 90 dB dynamic range, the detector consists of five stages, each with a dynamic range of 18 dB. This large total dynamic range is necessary because it has been shown by Matheson [19] that the APD of man-made radio noise may have a large dynamic range (e.g., 82 dB between the level exceeded 99% of the time and the level exceeded 0.01% of the time). The IF circuitry of the receiver used with the RNA will usually limit the dynamic range to less than 90 dB. The five outputs are each split into three levels each 6 dB apart. The digitizer consists of 15 fast acting comparators and some gating circuitry. One of the two inputs for each comparator is connected to a detector output and the other to an adjustable voltage source which sets the measurement threshold. In the APD mode, the output of each comparator is sampled with a very short aperture (130 nsec) at a specified sampling rate. As long as the detected IF envelope exceeds the comparator reference level, counts are added to the respective register at the sampling rate. In the ACR mode, each time the detected IF voltage exceeds a particular comparator reference level, only one count is added to the respective register (no matter

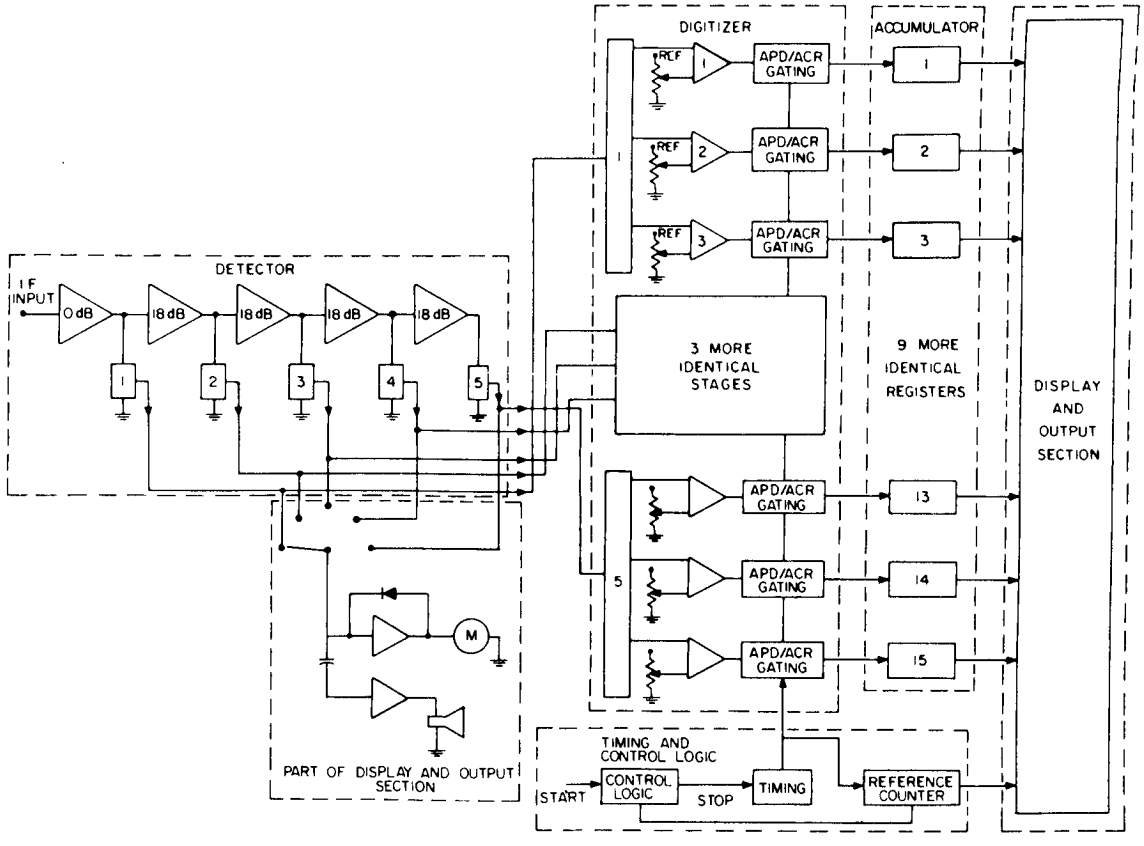

Figure 2. Block Diagram of Radio Noise Analyzer

how long the detected level stays above or below the comparator reference). Thus, one count is added for each positive transition. The accumulator consists of 15 registers each containing 10 cascaded decade counters. The timing and control logic produces the sampling pulses and controls the start and automatic stop of each distribution. The sampling rate is selectable in a 1,2,5 sequence from 2 KHz to 2 MHz. The number of samples for each APD distribution is selectable from 10^5 to 10^9. In the ACR mode, the combination of the sampling rate and number of samples is used to determine the length of time over which the ACR characteristic is measured. After a distribution is taken, the output of each register is displayed on a digital LED display and printed on a 16 digit Fluke printer.

The two Singer Meters were battery-powered but the remaining equipment was powered by a 300 watt Honda generator which was located 30 metres away from the measurement vehicle. The generator introduced no noticeable noise into the measurement data. This was checked by turning the generator off and on and watching and listening to the battery-powered meter for any change in noise levels.

2.3 HVDC POWERLINE

A description of this powerline and a large amount of background information regarding it may be found in the Proceedings of the National Power Conference EHV-DC held in July 1971 [20] at the time the line was put into service. The HVDC powerline consists of two bipolar circuits each on a single tower. These circuits may be operated in any combination of voltages up to ±450 KV in steps of 150 KV. The southern terminal of the line is Dorsey converter station. Figure 3 is a schematic of the powerlines around Dorsey. It also shows the relative location of the measurement sites described below. About 10 km north of Dorsey, a 230 KV AC powerline crosses the DC line and runs 100 metres parallel to it in the same right-of-way for a few hundred km. Figure 4 shows the DC line configuration near the converter station and Figure 5 shows the configuration at the Clarkleigh measurement site with the DC and AC lines both present

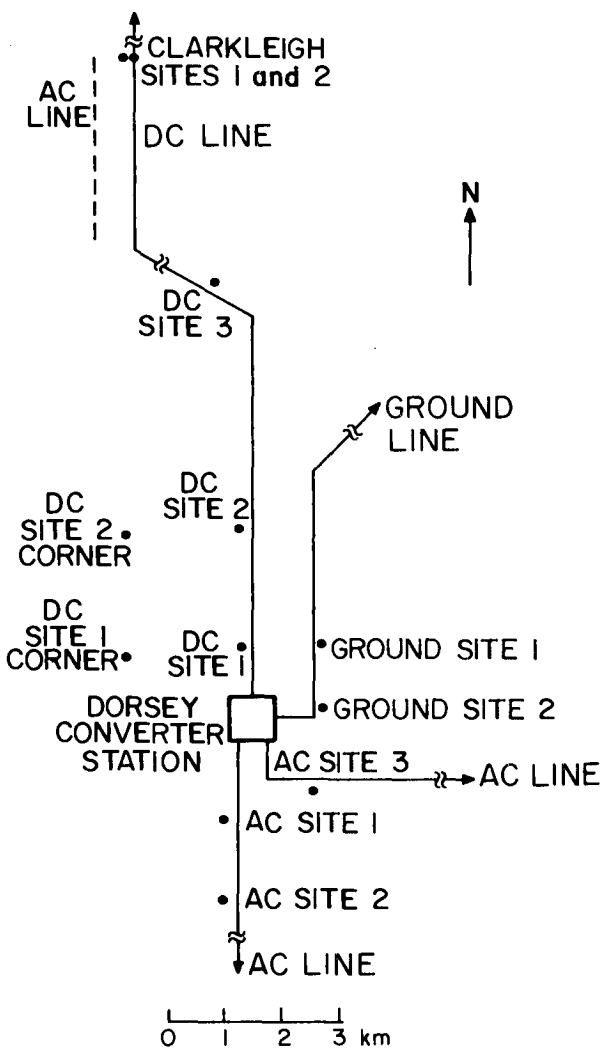

Figure 3. Locations of the Measurement Sites

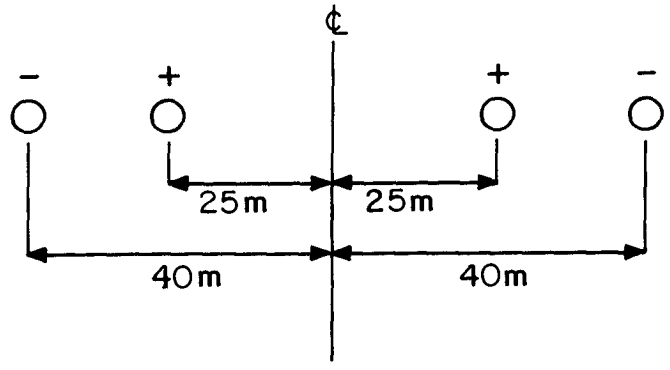

Figure 4. Configuration of the Powerline at Dorsey

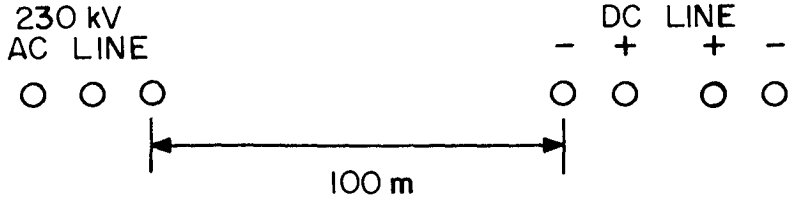

Figure 5. Configuration of the Powerline at Clarkleigh

2.4 MEASUREMENT SITES

The measurements were made on both the DC and the AC sides of the converter station. Figure 3 shows the relative locations of the measurement sites.

DC Site 1:

The measurements were made 15 and 30 m west of the outside conductor, 0.8 km north of Dorsey.

DC Site 2:

The measurements were made 15 m west of the outside conductor, 3.2 km north of Dorsey.

DC Site 3:

The measurements were made 15 m east of the outside conductor, 8 km north of Dorsey.

AC Site 1:

The measurements were made 15 m west of the outside conductor, 1.6 km south of Dorsey.

AC Site 2:

The measurements were made 15 m west of the outside conductor, 3.2 km south of Dorsey.

AC Site 3:

The measurements were made 15 m south of the outside conductor, 0.8 km south-east of Dorsey.

Clarkleigh 1:

The measurements were made between the DC and 230 kV AC line at a location 15 m west of the outside conductor of the DC line, 80 km north of Dorsey.

Clarkleigh 2:

The measurements were made midway between the two DC circuits, 80 km north of Dorsey.

DC Site 1 corner:

The measurements were taken 2.4 km west of Dorsey and 0.8 km north.

DC Site 2 corner:

The measurements were taken 2.4 km west and 3.2 km north of Dorsey.

Ground Site 1:

The measurements were taken 15 m east of the ground line, 0.8 km east and 0.8 km north of Dorsey.

Ground Site 2:

The measurements were taken 15 m east of the ground line, 0.8 km east of Dorsey.

2.5 MEASUREMENTS

The tests discussed in this report consisted of V_{rms}, V_d, V_{qp}, APD and ACR measurements taken during fair weather conditions over a one week period in July 1977. Table 1 shows the location, date, powerline condition and frequency range for each of the 21 separate tests. The tests were numbered in chronological order. They produced 125 pairs of APD and ACR data. The number of pairs of distributions from each test is shown in the last column of Table 1. Each APD consisted of 10^6 samples taken at a sampling rate of 20 KHz (a measurement time of 50 seconds). Each ACR was taken over a time period of 100 seconds.

The basic procedure followed for the tests at each measurement frequency was: (1) measure V_{rms} and V_d with the NM-26T, (2) then attach the antenna to

TABLE 1

Summary of Available Data

Measurement Site	Test No.	Date (1977)	Powerline Parameters	Frequency Range (MHz)	No. of Distributions
DC Site 1 (15m)	1	July 23	±150KV (550A)	1.1 to 10.0	—
	2	July 23	$\begin{cases}-450\\+300\end{cases}$KV (700A)	2.0 to 5.0	6
	4	July 24	OFF	1.1 to 10.0	7
	7	July 24	±300KV (670A)	1.1 to 10.0	3
	8	July 25	±300KV (500A)	1.1 to 10.0	13
	11	July 25	$\begin{cases}-300\\+150\end{cases}$KV (1320A)	1.5 to 5.0	2
	* 18A	July 27	±300KV (1140A)	1.5 to 10.0	6
	** 21	July 28	±450KV (800A)	1.1 to 10.0	16
DC Site 1 (30m)	12	July 25	$\begin{cases}-300\\+150\end{cases}$KV (1320A)	1.5 to 5.0	3
	* 18B	July 27	±300KV (140A)	1.5 to 10.0	7
DC Site 2	3	July 23	$\begin{cases}-450\\+300\end{cases}$KV (780A)	1.1 to 2.0	6
	9	July 25	±300KV (1000A)	1.1 to 10.0	7
DC Site 3	10	July 25	±300KV (1000A)	1.1 to 5.0	8
DC Ground Site 1	19	July 27	$\begin{cases}-450\\+300\end{cases}$KV (920A)	1.5 to 10.0	5
DC Ground Site 2	20	July 27	$\begin{cases}-450\\+300\end{cases}$KV (920A)	1.5 to 10.0	5
DC Site 1 Corner	16	July 27	±150KV (400A)	1.5 to 10.0	—
DC Site 2 Corner	17	July 27	±150KV (400A)	1.1 to 10.0	5
Clarkleigh 1	13	July 26	$\begin{cases}-450\\+300\end{cases}$KV (900A)	1.1 to 5.0	5
Clarkleigh 2	14	July 26	$\begin{cases}-450\\+300\end{cases}$KV (900A)	1.1 to 5.0	2
AC Site 1	5	July 24	±300KV (500A)	1.0 to 10.0	8
AC Site 2	6	July 24	±300KV (500A)	1.1 to 5.0	1
AC Site 3	15	July 26	$\begin{cases}-450\\+300\end{cases}$KV (810A)	1.1 to 10.0	10

NOTES: * *The measurements were made alternately at distances of 15 and 30 meters.*

** *The noise was predominately DC corona at this voltage level.*

the NM-25T and measure V_{qp}, (3) return the antenna to the NM-26T and set the function switch to PEAK (fixed AGC) and take an APD measurement, (4) check V_{rms} and V_d for any change in the noise level or characteristic and then, if the APD was taken correctly (i.e., within the dynamic range of the RNA - no overloads or set noise measurements), (5) measure the ACR and finally (6) check V_{rms}, V_d and V_{qp} for any change (stationarity) before going on to the next frequency. This was the procedure followed for most of the tests, however, in two of the tests [1 and 16], measurements were only made of V_{rms} and V_d.

3. ANALYSIS

3.1 INTRODUCTION

Most of the measurements were taken at a distance of 15 metres from the outer conductor (except tests 12, 16, 17 and 18b). Lateral profiles of the powerline were not attempted except that some measurements (tests 11, 12 and 18) were taken at 30 metres from the powerline. No significant differences were found between the 15 and 30 metre measurements, consequently the results of the V_{rms}, V_d and V_{qp} data will be presented only as a function of frequency. The analysis is divided into three subsections: (1) presents the V_{rms}, V_d and V_{qp} measured data, (2) presents the calculated values of V_{rms}, V_d and V_{qp}, (3) presents the APD data and (4) presents the ACR data.

3.2 MEASURED V_{rms}, V_d and V_{qp} DATA

V_{rms} is a measure of the average power radiated from the powerline. The effective antenna noise figure, F_a, is the preferred way of expressing the average noise power from sources external to the antenna and is defined by:

$$F_a = 10 \log f_a \tag{1}$$

where

$$f_a = p_n / kT_o b; \tag{2}$$

p_n is the received noise power, in watts, available from an equivalent loss-free antenna (i.e., power available after correction for antenna losses) in a noise power bandwidth b, in hertz, k is Boltzmann's constant, 1.38×10^{-23} joules/Kelvin, and T_o is the reference temperature, 288K. The quantity f_a is dimensionless (the ratio of two powers) but it gives, numerically, the available power spectral density relative to kT_o and the available power relative to $kT_o b$. Thus, F_a is defined in units of dB above kT_o or dB above $kT_o b$.

For a short vertical antenna over a perfect ground and a reference temperature T_o = 288 K (15°C), F_a is given by [9]:

$$F_a = E_n - 20 \log F + 95.5 - 10 \log b \tag{3}$$

where E_n is the measured rms field strength of the vertical component of the noise field (in dB above 1 μV/m) for a noise power bandwidth b. F is the

received frequency (MHz). E_n is defined by:

$$E_n = MR + AF + CL \tag{4}$$

where MR is the rms meter reading (dB above 1 μV),

CL is the antenna cable loss (dB) for the 20 feet of RG58 used to connect the antenna coupler to the receiver, and

AF is the antenna figure which is made up of two parts:

$$AF = CF - EH$$

where CF is the coupler insertion loss factor (dB) determined from a set of calibration curves supplied with the antenna coupler and EH is the antenna effective height (dB above 1 metre . The effective height of a vertical monopole less than λ/10 in physical height above an infinite, perfectly conducting ground plane is equal to one-half the physical height. For the 9 foot rod, the effective height figure, EH, is 20 log (9/2 x 0.3048) = 2.7 dB above 1 metre.

Combining 3 and 4, we have

$$F_a = MR + K_f \tag{5}$$

where K_f is a combined factor having a different value for each frequency

$$K_f = 95.5 - 10 \log b - 20 \log F + CF - EH + CL \tag{6}$$

The effective noise power bandwidth, b of the Singer NM-26T receiver is taken as 4 KHz. (See Table 1 of discussion by Hagn and Shepherd of "A Field Comparison of RI and TVI Instrumentation" [1].)

The Voltage deviation (V_d) is a measure of the impulsiveness of the noise process. It is defined as the difference in dB between the RMS and average noise envelope voltages.

The quasi peak data is usually presented as dB above 1μv/metre and is called by powerline people RI (Radio Interference level). The RI values shown in Appendix A were calculated from the following.

$$RI(\text{dB above 1 } \mu v/m) = MR + AF + CL \tag{7}$$

where the terms are defined above (after equation 4) for the V_{rms} to F_a computations.

The quasi peak measurements were made with the Singer NM-25T which uses the ANSI time constants (1 ms charge and 600 ms discharge) and a 6 dB bandwidth of 4.5 KHz.

Appendix A presents the values of F_a, V_d and $RI(V_{qp})$ from the 21 tests. In this section, linear regression lines are presented to show typical levels and frequency functions of the data.

Figure 6a shows the F_a levels for the "line off" test (No. 4). Even with the HVDC powerline shut down, there was still a significant amount of powerline noise in the area. This is shown by comparing the OFF test results with the CCIR expected values of man-made noise at a "rural" location [21]. The measured levels were 13 to 5 dB higher varying with frequency than the rural prediction. The results for the area, i.e., not adjacent to the line area are also shown on this figure (tests No. 16, and 17). These values were measured 1.6 km from the line when the converter valves were the dominant source of noise. Note also the steep slope (-50 dB/decade) as compared with the CCIR prediction (-27.7 dB/decade). This rapid decrease in levels as a function of frequency seems to be characteristic of noise from this powerline as is shown in Figure 6b. In this figure, the measurements at Clarkleigh (Tests No. 13 and 14) located 80 km north of Dorsey are shown. The measurements for the DC side of the converter station (Tests No. 1,2,3,7,8,9,10,11, 18A,19 and 20) have been combined. Even though these measurements were taken at a number of sites and powerline voltage conditions, there was not a significant spread in their level (no discernable trend). The same situation was found for the measurements on the AC side of the converter station (Tests Nos. 3, 6 and 15). The AC side levels are higher because the noise at these sites was a combination of the valve noise and AC hum. This figure also shows the measurement for the DC corona (test No. 21). In this case, the noise is a combination of the converter valve noise and the DC corona with the corona being the dominant source. Aurally, it drowned out the valves. The four measurement lines show a very rapid fall-off in levels as a function of frequency (some -50 to -60 dB/decade) as compared to the CCIR man-made noise prediction (-27.7 dB/decade). The DC corona measurements were 39 to 16 dB varying with frequency above the CCIR rural line and 28 to 6 dB above the CCIR business line [21].

Figures 7a and b show regression lines for the V_d measurements using the same groupings as used in Figure 6. The limiting value for V_d is 1.05 for gaussian noise. Figure 7a also shows the expected median values of V_d for a rural area [22]. The area line falls below this but the OFF line test measurements for frequencies below 5 MHz shows a very impulsive noise process. Figure 7b shows that the noise levels at Clarkleigh are not very impulsive. The actual measured values limited at 1.05 dB for higher frequencies and the regression line was based only on the data below 2.5 MHz. The DC side measurements were the most impulsive because they were from the converter valve noise. The AC side was less impulsive because of the periodic component of the AC hum which tends to lower the V_d value. Although the DC corona had the highest F_a values, it is much less impulsive because the corona noise results from a large number of sources, that by the central limit theorem tend to produce gaussian noise. The presence of the valve noise kept the V_d value above the gaussian limit. From these two figures, it can be seen that there is a very small frequency effect; i.e., the slopes of the lines are about -1 to -2 dB/decade. This shows that for each of the measurements, the dominant noise process remained the same over the 1-10 MHz frequency range.

Figures 8a and b show regression lines for the RI values using the same data groupings as used in Figure 6. In Figure 8a, it is shown that the area line is higher than the OFF one, similar to Figure 6a for the F_a values. Also, the relative levels in Figure 8b for the DC corona, AC side, DC side and Clarkleigh are similar to those shown in Figure 6b. An important point to note here is that the slopes of the RI lines range from -30 to -40 dB/decade;

i.e., they fall off much slower than the average power levels (20 dB slower). These results also compare with those of Morris et al [5] who found that the DC corona values vary with frequency at a rate of -30 dB/decade.

3.3 CALCULATED V_{rms}, V_d and V_{qp} DATA

As stated in Section 1, one of the objectives of these tests was to study the accuracy of computing V_{rms}, V_d and V_{qp} from APD data. From a very limited number of examples, it has been shown [2] that it is possible to calculate values of V_{rms} and V_d from the APD data using the following equations.

$$V_{average} = -\sum_{i=1}^{N-1} V_i \Delta P_o(v_i) \text{ volts} \tag{8}$$

$$(V_{rms})^2 = -\sum_{i=1}^{N-1} V_i^2 \, \Delta P_o(v_i) \text{ volts}^2 \tag{9}$$

where $V_i = v_i + \Delta v/2$

v_i is the i^{th} level threshold voltage (volts) and $v_{i+1} > v_i$.

$\Delta v = v_{i+1} - v_i$

$\Delta P_o(v_i) = P_o(v_{i+1}) - P_o(v_i)$.

$P_o(v_i)$ is the measured probability that the i^{th} threshold value is exceeded.

N is the total number of threshold levels for which we have $P_o(v_i)$ data.

$$V_d = 10 \log (V_{rms})^2 - 20 \log (V_{average}) \text{ dB} \tag{10}$$

Cook has recently published a paper [23] that describes how to calculate V_{qp} from APDs. In this paper, he tested his equations to a large extent with the data given in reference 2. There is much interest in obtaining values of the v_{qp}/v_{rms} ratio (defined as $Q_d = 20 \log v_{qp}/v_{rms}$ [24]) for man-made radio noise processes since most of the published data to date especially from powerline noise is in terms of V_{qp}, whereas, the parameters required to determine the effects of noise on most modern communication systems must be statistical (e.g., v_{rms}, etc).

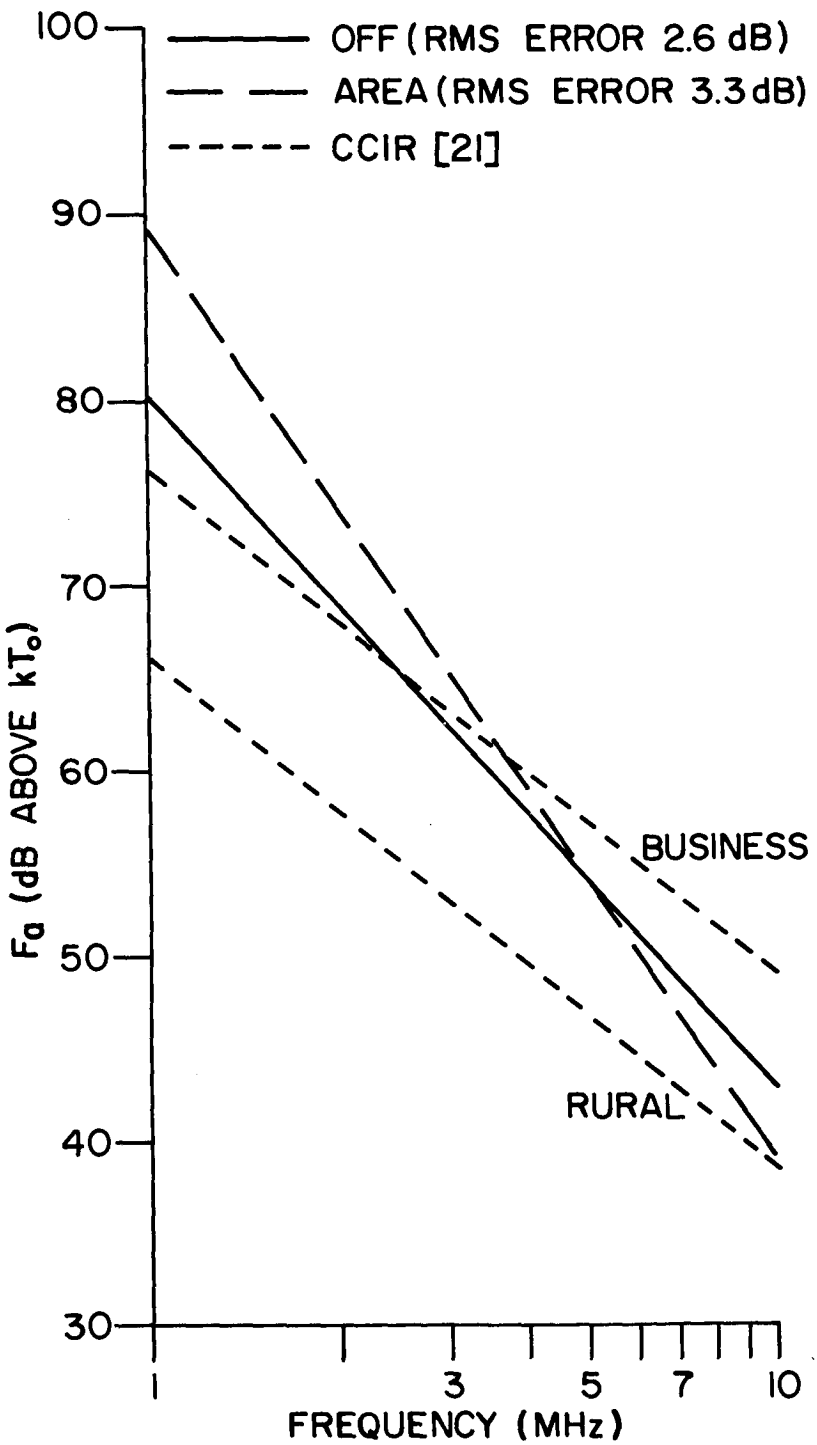

Figure 6(a). Regression Lines of F_a Versus Frequency

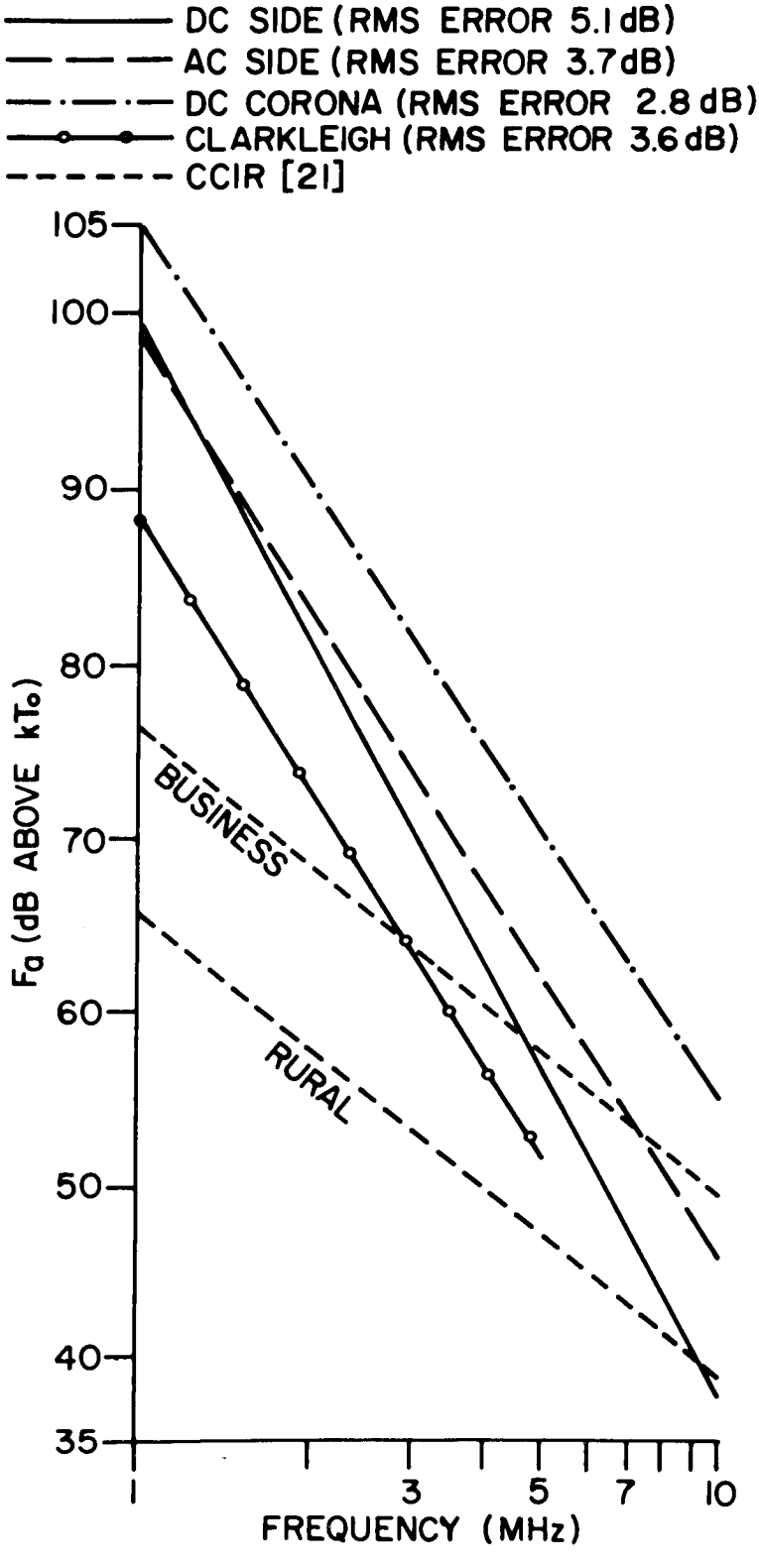

Figure 6(b). Regression Lines of F_a Versus Frequency

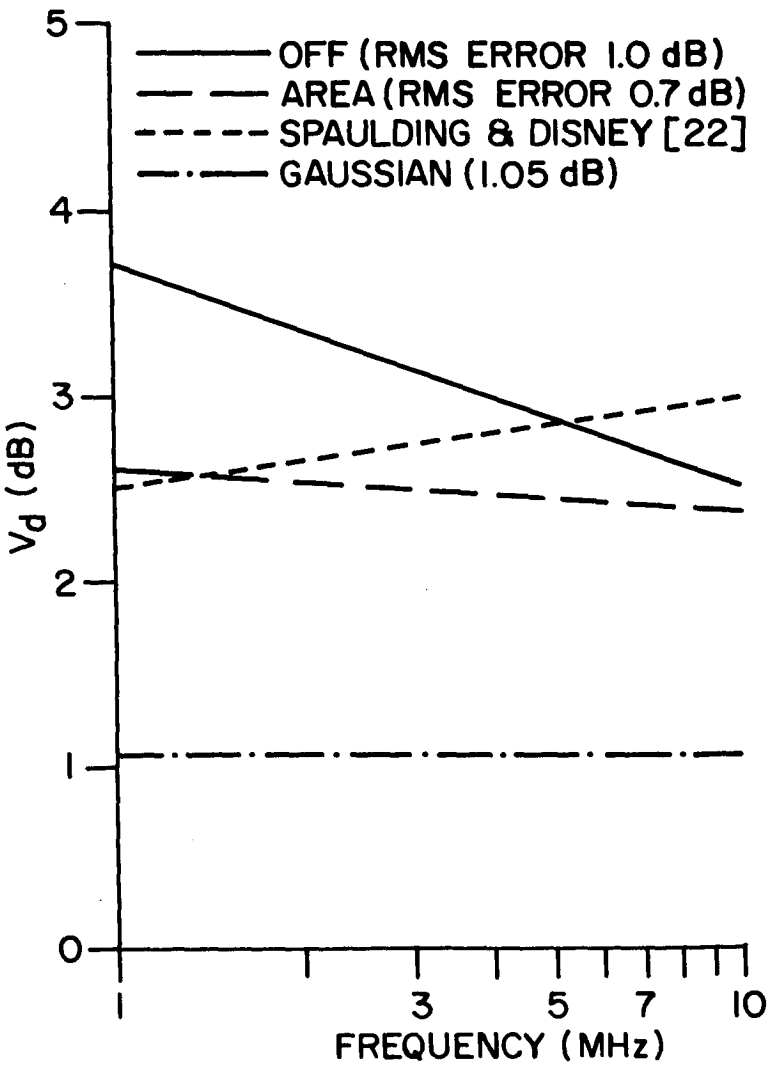

Figure 7(a). Regression Lines of V_d Versus Frequency

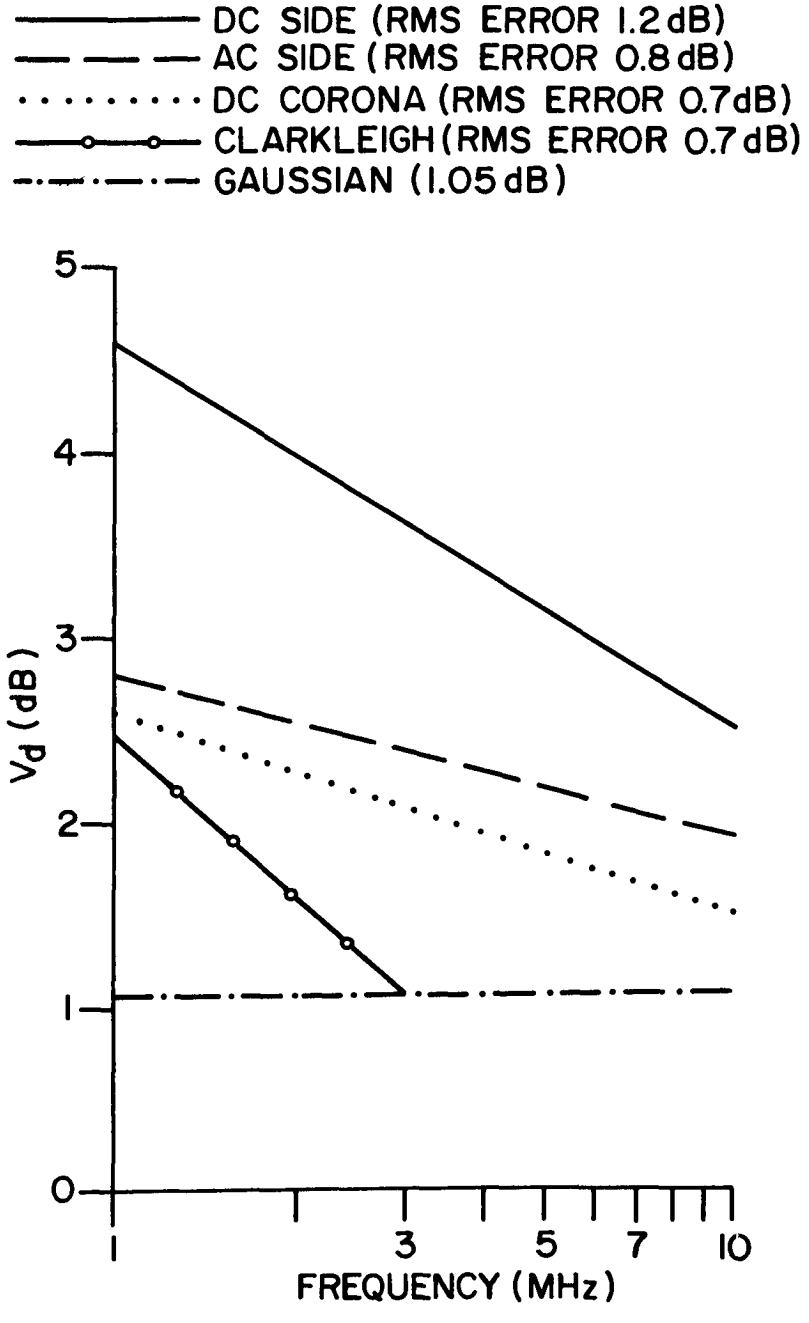

Figure 7(b). Regression Lines of V_d versus Frequency

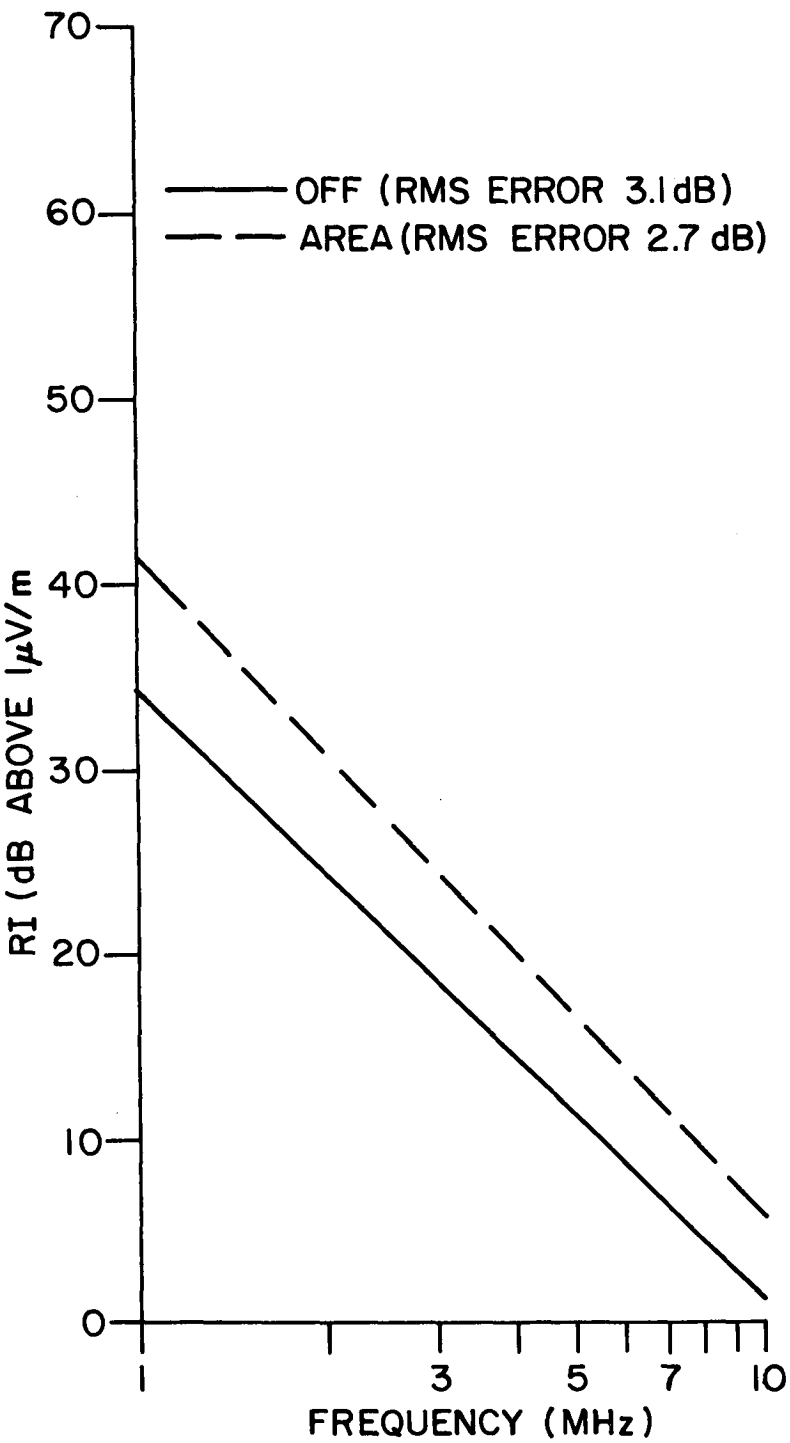

Figure 8(a). Regression Lines of V_{qp} Versus Frequency

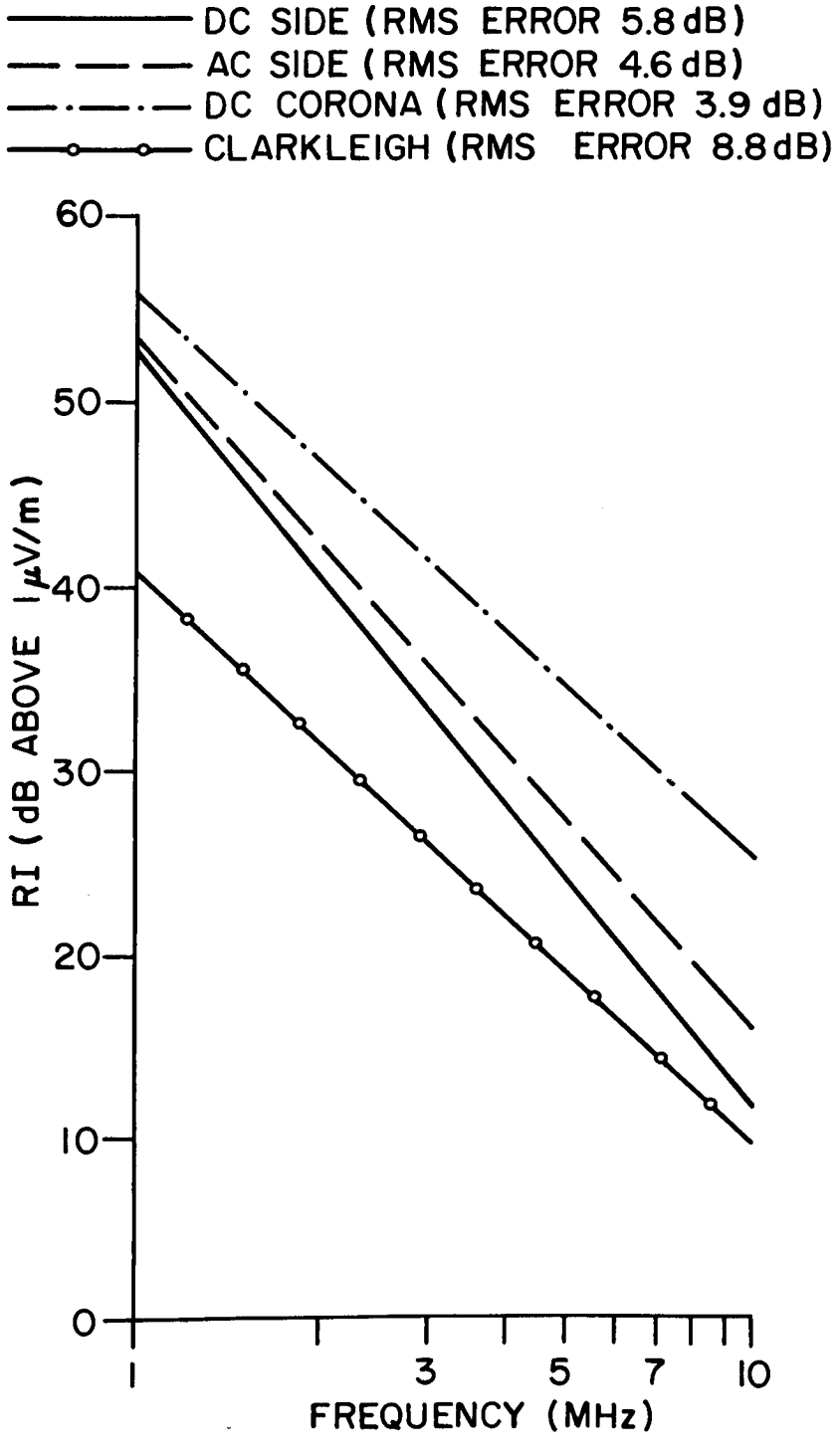

Figure 8(b). Regression Lines of V_{qp} Versus Frequency

Values of Q_d may be calculated from the APD data. Let $q_d = v_{qp}/v_{rms}$ where $Q_d = 20 \log g_d$. Thus, using the following (Cook's equations 3 and 8)

$$q_d = R_D/R_C \int_{q_d}^{\infty} (e - g_d) p_e(e) de \tag{11}$$

$$\text{where } p_e(e) = \frac{1}{\pi} \int_{e}^{\infty} \frac{\frac{-dP(A)}{dA}}{\sqrt{A^2 - e^2}} \tag{12}$$

R_D/R_C = 2400 for the ANSI time constants of 1 ms charge and 600 ms discharge.

P(A) is the relative APD/ i.e., all levels (A) are relative to V_{rms} and e is a random variable representing the instantaneous IF voltage.

The measured Q_d were obtained by subtracting V_{rms} measured with the NM-26T from the V_{qp} measured on the NM-25T*. The relative APD is obtained by computing V_{rms} from the APD data and then referencing the APD values to this level.

Figure 9 shows the correlation between the measured and calculated values of V_{rms}, V_d and Q_d. As shown, there is a good degree of correlation r = 0.98 for V_{rms}, 0.79 for V_d and 0.58 for Q_d. From the 125 samples, it was possible to produce a cumulative distribution of the difference between the calculated and measured values for the three parameters (difference = calculated value - measured value) as shown in Figure 10. Table 2 summarizes these results and compares the differences with the measurement accuracy of the equipment.

This shows that it is possible to calculate accurate values of V_{rms}, V_d and Q_d from the APD data.

As mentioned previously, there is much interest in obtaining values of Q_d for man-made radio noise processes since most of the data published to date, especially from powerline noise, is in terms of V_{qp}. From these tests, it is possible to group the data for three separate man-made noise processes for estimating values of Q_d. Group One consisted of the 16 APDs from Test No. 21. The noise was a composite of DC corona and valve noise with the corona being predominant. Group Two consisted of the 19 APDs from Tests Nos. 5, 6 and 15. These were measured on the AC side of the converter where the noise was a composite of AC hum and valve noise. Group Three consisted of the 71 APDs from Test Nos. 2,3,7,8,9,10,11,12,18,19 and 20. These were measured on the DC side of the converter where the noise was basically valve noise. Table 3 shows the results of the three groups for both measured and calculated

---

* *When these measurements were made there was no commercially available instrument to measure Q_d directly, however, Electrometrics division of Penril Corp. has developed an instrument termed a CRM-25 for use with the EMC-25 Mark III field intensity meter which will measure Q_d directly.*

Q_d values. These results show that a value of 12 dB ± 2 dB is quite realistic for these types of man-made radio noise. This result is consistent with Cook's limited sample. The values of the standard deviations are of the same order as the accuracy of most meters used for making these measurements.

TABLE 2

Results From Cumulative Distributions

Parameter	Median Difference (dB)	Decile Values* (dB)	Measurement Accuracy** (dB)
V_{rms}	0.6	+3 −1	±2
V_d	0.2	±1	±1
Q_d	0.1	±2	±4

* *Those exceeded 10% and 90% of the time.*

** *The accuracy of setting the APD threshold ±1 dB.*

TABLE 3

Results of Measured and Calculated Q_d Values

Description	Median Q_d (dB)	σ (dB)	D_u (dB)	D_1 (dB)
Measured Q_d from DC corona*	11.0	2.1	2.5	2.5
Calculated Q_d from DC corona (16 APDs)	11.6	2.5	1.8	5.6
Measured Q_d from AC*	10.5	1.9	3.5	2.5
Calculated Q_d from AC (19 APDs)	11.2	1.9	1.3	2.5
Measured Q_d from DC Valves*	12.5	2.2	2.5	3.5
Calculated Q_d from DC Valves (71 APDs)	12.4	1.8	2.1	2.3

where σ = standard deviation

D_u = ratio of the upper decile (value exceeded 10% of time) to the median expressed in dB.

D_1 = ratio of the median to lower decile (value exceeded 90% of the time) expressed in dB.

* *The measurement values used were those that were associated with the APDs used for the calculated values.*

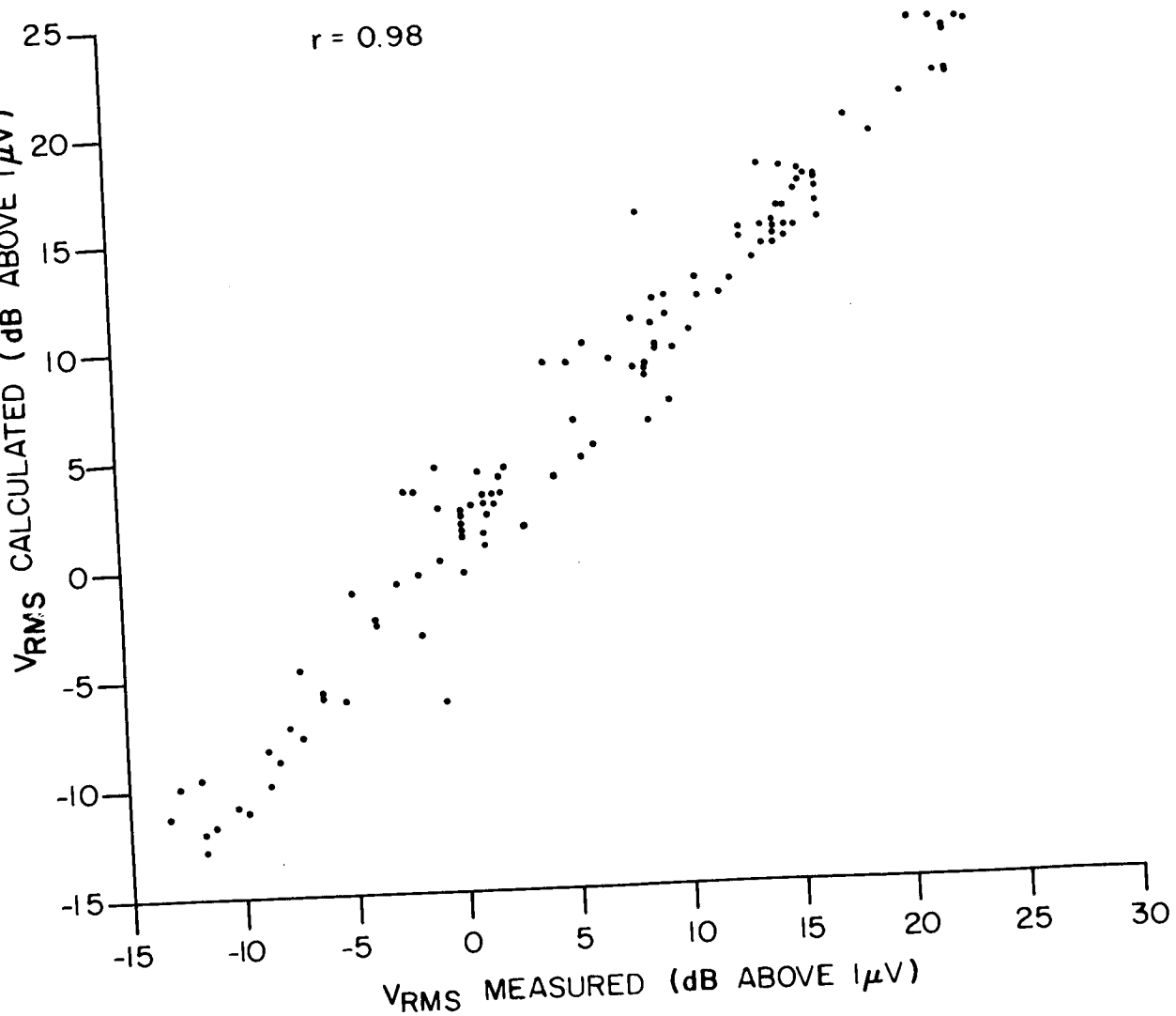

Figure 9(a). Correlation of Measured and Calculated V_{rms} Values.

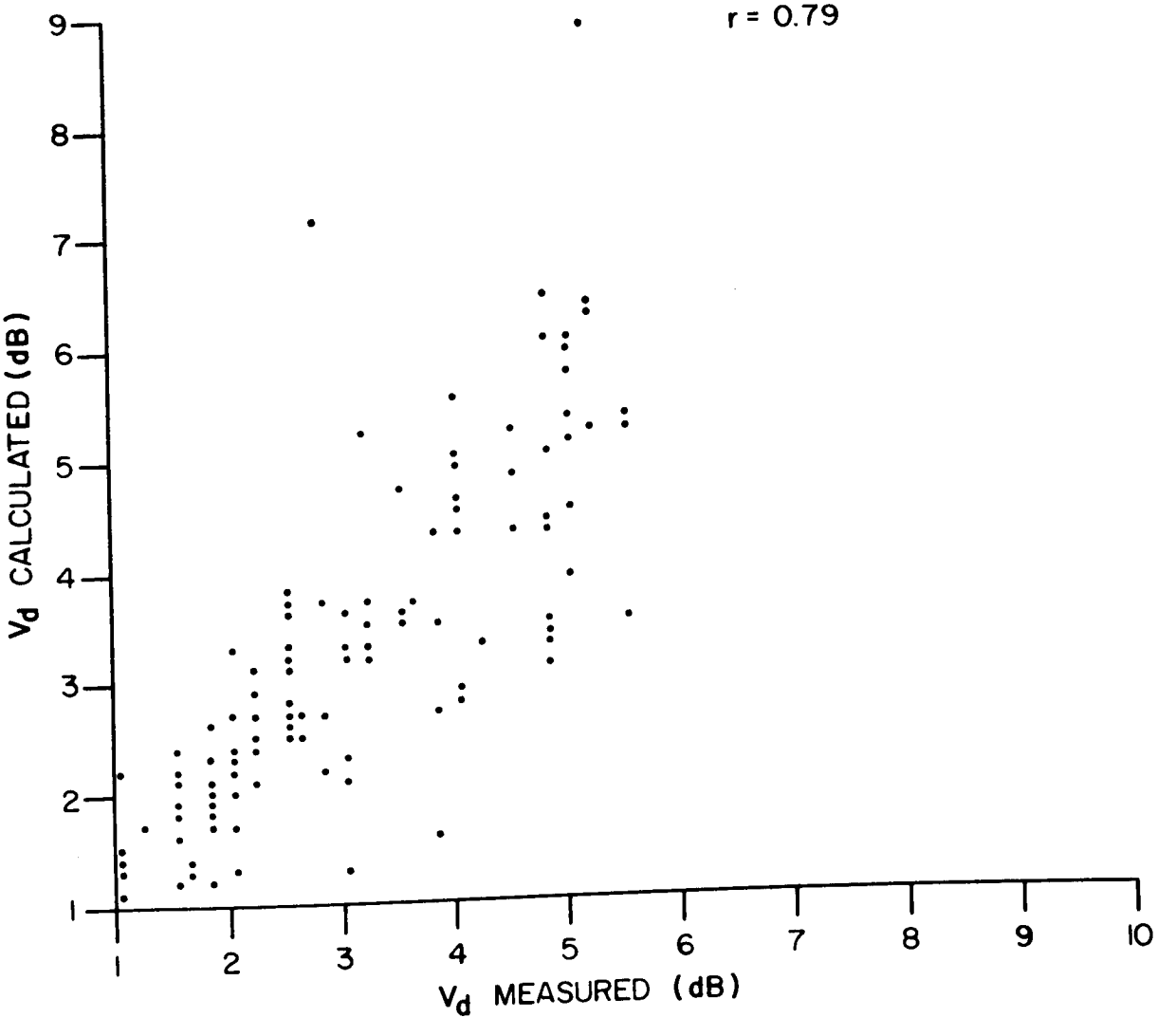

Figure 9(b). Correlation of Measured and Calculated V_d Values

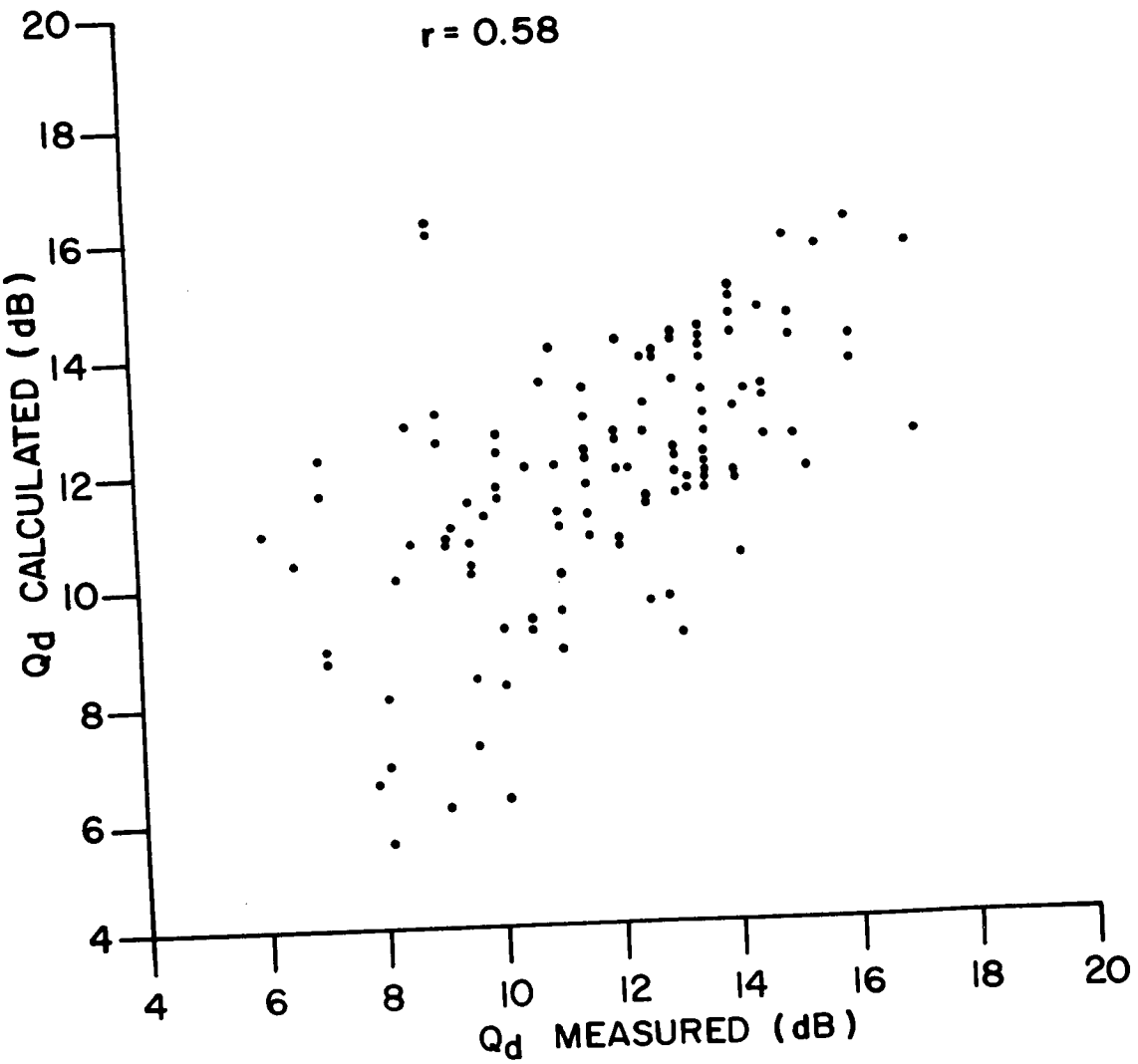

Figure 9(c). Correlation of Measured and Calculated Q_d Values

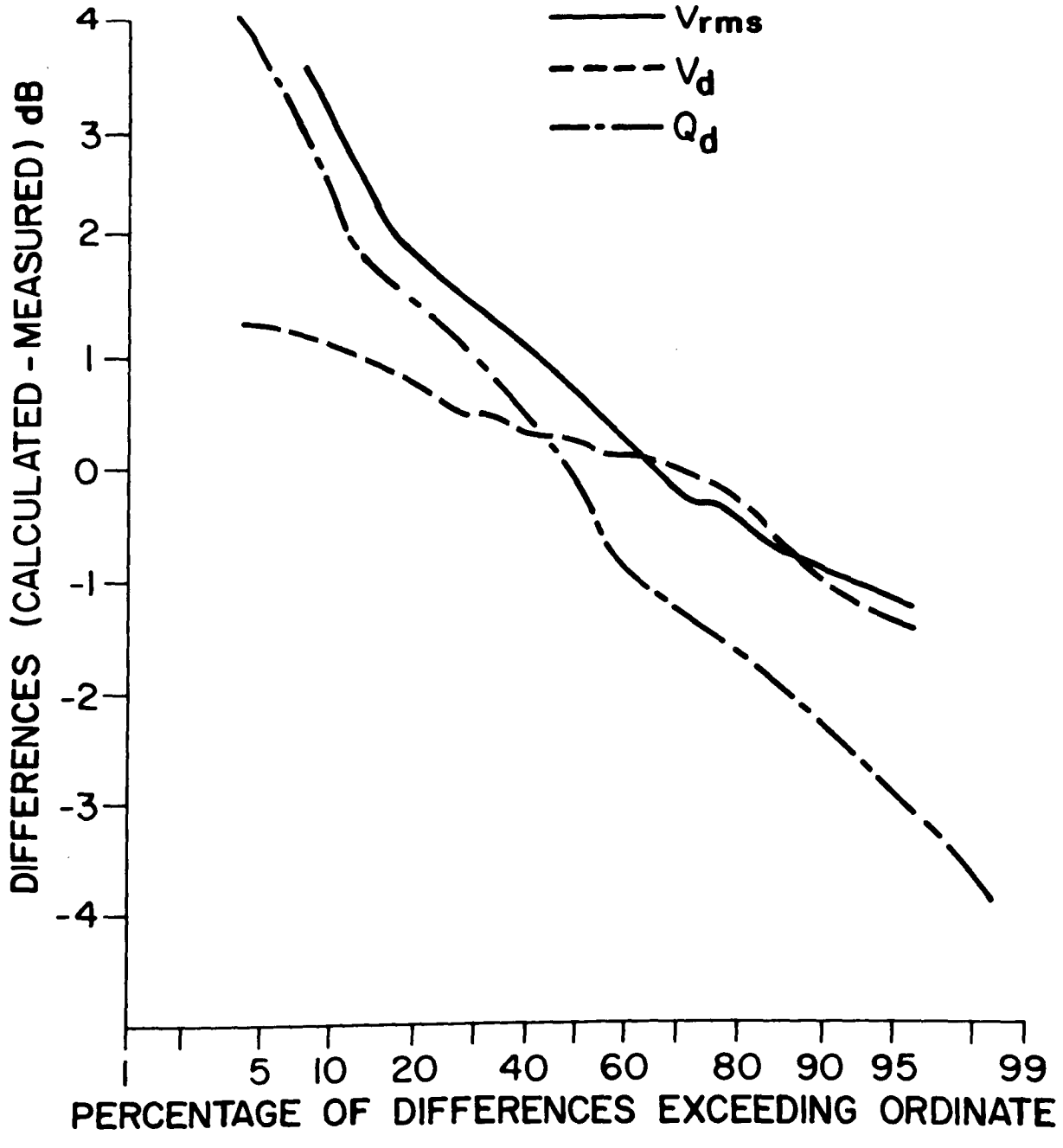

Figure 10. Cumulative Distribution of the Differences Between the Calculated and Measured Values of V_{rms}, V_d and Q_d.

3.4 APD DATA

A further objective of these tests was to study the suitability of applying widely used mathematical models, developed for atmospheric noise, to man-made radio noise. This involves predicting the APD and ACR from measurements of V_{rms} and V_d used as inputs to a suitable mathematical model. Since most engineers do not want to have to make sophisticated statistical measurements, it is desirable to be able to take basic measurements and from them to predict, reliably, the statistical distributions which in turn may be used to predict the performance of communication systems.

The recently developed, very powerful statistical-physical models of Middleton [25,26,27,28] have not yet been simply related to basic measurement parameters; i.e., one must vary the model parameters for a best fit or know specifically the source characteristics which, in most man-made radio noise measurements are very difficult to define. Powerline noise and most man-made radio noise are usually considered broadband. Middleton calls this Class B noise where the noise is generated by sources whose emission spectra are much broader than the bandpass of the receiver.

A good summary of the models developed up to the mid]970's is given by Spaulding and Middleton [29]. Most models fit one of two categories. The first category is termed experimental where the model is based totally or partially on measured statistics (empirical models). These models do not represent the noise process but are merely mathematical expressions to fit the measured statistics. They usually only consider the first order envelope statistics and are not capable of predicting higher order statistics. The second category is termed theoretical. These models are derived from the physical noise processes and use measurements as a check on their accuracy. A few models have started as empirical and have been subsequently given theoretical support, e.g., the Log-Normal model.

The Rayleigh, Atmospheric, Log-Normal and Hall models are used in this report. These four models were chosen because they are typical of the models used today to determine the performance of digital communication systems and to solve detection problems and the parameters are related to the basic measurement parameters, V_{rms} and V_d. This will also test the suitability of applying atmospheric noise models to various types of man-made noise.

The simplest model is to assume that the noise is Gaussian. In this case, the envelope is Rayleigh distributed [30] and the APD is given by:

$$P_o(V) = e^{-V^2/V_{rms}^2} \tag{13}$$

Since the Gaussian noise assumption is used very often in communication system performance predict, it was necessary to check if these man-made noise processes were Gaussian. Also this model gives a reference with which to compare the other models.

The second model that was considered is termed the Atmospheric noise model. It was one of the first modelling procedures to be used and was developed by Crichlow et al. in 1960 [31]. Their empirical model (based on

a geometrical construction) consisted of two straight lines (one for the Rayleigh component and one for the impulsive component) joined by a circular section. It used values of V_d and L_d (dB difference between the rms and log noise envelope voltages) to give the characteristic shape of the relative APD (relative to V_{rms}). L_d was subsequently found to be linearly related to V_d by Spaulding et al in]962 [32]. The resulting family of curves was first published in]962 [32] and subsequently in CCIR Report 322 [9] in]963 with only the V_d parameter determining the shape. These curves have found wide usage. In]972, Akima published a computer program to generate this model as well as a random number generator program for use in simulation studies [33]. The APD function in Akima's report is defined by the subroutine APDAN:

$$P_o(V) = \text{APDAN}(V_d, K, \text{DDB}) \tag{14}$$

where V_d is the ratio of rms to average envelope voltage (dB).

K = 1 for the APD function

2 for the probability density function

DB = the envelope voltage (dB relative to V_{rms}) for which the APD or density function is computed.

The simplicity, accuracy and the computer programs of Akima have lead this model to be the "standard" representation for atmospheric noise and it has generally been used in determining the performance of digital systems in atmospheric noise. The biggest disadvantage of the model is that it only addresses the APD of the receiver noise envelope and does not consider the temporal statistics. The model also does not relate to the physical processes involved.

In 1964, Beckmann developed a theoretical model for the received waveform of atmospheric noise and was the first to relate the model to the physical process generating the noise (number of sources, propagation properties). This model proposes that the noise envelope of the received noise is Rayleigh distributed at low levels and Log-Normally distributed at high levels [34]. In 1969, Omura further developed the Log-Normal part of this model and derived relationships between this model and measurable quantities (V_{rms} and V_d) [14]. Moreover, he was able to derive expressions for the ACR and Pulse Spacing Distributions; i.e., he was able to model the temporal as well as the amplitude characteristics of the noise. The advantage of this model over the atmospheric one is this ability to model the temporal characteristics of the noise and its much stronger theoretical basis.

The Log-Normal model assumes a noise envelope of the form:

$$V(t) = Ce^{n(t)} \tag{15}$$

where n(t) is a zero-mean Gaussian random process with variance σ_n^2. Omura showed that the APD is given by:

$$P_o(V) = 1 - \psi(\alpha) \tag{16}$$

where

$$\psi(\alpha) = \frac{1}{2\pi}\int_{-\infty}^{\alpha} e^{-x^2/2}\ (dx) \quad \text{(standard normal function)}$$

$$\alpha = \frac{\ln\ (V/C)}{\sqrt{\sigma_n^2}} \tag{17}$$

$$\sigma_n^2 = \frac{V_d}{10\ \log\ e} \tag{18}$$

$$C = \frac{V_{rms}}{e^{\sigma_n^2}} \tag{19}$$

The Hall model was the final model to be considered. In 1966, Hall proposed that the received noise was a narrowband Gaussian process multiplied by a weighting factor that varies with time [15], i.e.,

$$V(t) = a(t)n(t) \tag{20}$$

where n(t) is a zero-mean Gaussian process and a(t) is a stationary random process independent of n(t). For this model, he was able to develop expressions for the APD, ACR and distribution of pulsewidths and pulse spacings. The APD is given by

$$P_o(V) = \frac{\gamma^{(\theta-1)}}{(V^2+\gamma^2)^{(\theta-1)/2}} \tag{21}$$

where θ and γ are the model parameters. Hall relates his model to basic radio parameters (V_{rms} and V_d) for $\theta = 3$ and $\theta = 4$. For $\theta = 4$, the V_d is fixed and there are no possible model variations, thus, $\theta = 3$ was used for this test. In this case

$$\gamma = \frac{2}{\pi} V_{average} \tag{22}$$

and

$$V_{average} = 10^{(V_{rms}-V_d)/20} \tag{23}$$

One problem with this model is that for $\theta=3$, V(t) has an infinite variance; thus the model does not apply to a real physical process. Schonhoff et al. [35] proposed a truncated Hall model in 1977 to eliminate this problem. Girodano,

in 1970, [16,36] gave a theoretical explanation for the Hall model and related the model parameters θ and γ to the physical process.

To date, few measures of fit have been developed for comparing the performance of several models. Typically, in the literature one will find an APD graph like Figure 11 showing measured data and a model curve through it. Sometimes a Rayleigh curve is drawn for contrast to show that the measured data fits the model curve rather than the Rayleigh curve. However, this does not really present a quantitative measure of fit between the models and the measured data. There is a statistical measure of fit called the Kolmogonov-Smirnov one sample test which could be used [37]. It determines whether a set of samples can be reasonably thought to have come from a population having a given theoretical distribution. The test involves specifying the cumulative distribution (or APD) which would occur under the theoretical distribution and comparing it with the observed cumulative distribution (or APD). The point at which these two distributions, theoretical and observed, show the greatest difference is determined.

$$D = \text{MAXIMUM } |S(X) - F(X)|$$

where F(X) is the theoretical cumulative distribution (or APD) and

S(X) is the observed cumulative distribution (or APD).

Reference to a sampling distribution indicates whether such a large divergence is likely on the basis of chance. In our case for 10^6 samples per distribution

$$D = 1.63/\sqrt{N} = 0.163\%$$

is the maximum allowed difference at the 1% significance level.

This test proved too strong for our data since even for the best model only 4 distributions come within an order of magnitude (i.e., 1.6%) of reaching this difference.

The maximum difference occured in the centre of the APDs and the smallest difference occurred at the tails of the distributions.

The measure of fit used in this report was the RMS DIFFERENCE between the model and measured APD data given by the following expression.

$$\text{RMS DIFFERENCE} = \sqrt{\frac{\sum_{i=1}^{N} [P_o(V_i)_{\text{model}} - P_o(V_i)_{\text{measured}}]^2}{N}} \quad \% \qquad (24)$$

This is illustrated in Figure 12 which shows some typical APD data and a model curve. As shown above (equations 13, 14, 16 and 21), each of the models output probability values (%) from inputs of relative APD levels. Thus, we perform an RMS DIFFERENCE on the probabilities. This seems to be

the best measure of fit since the largest differences between the models and the measured data occurred in the centre of the distributions.

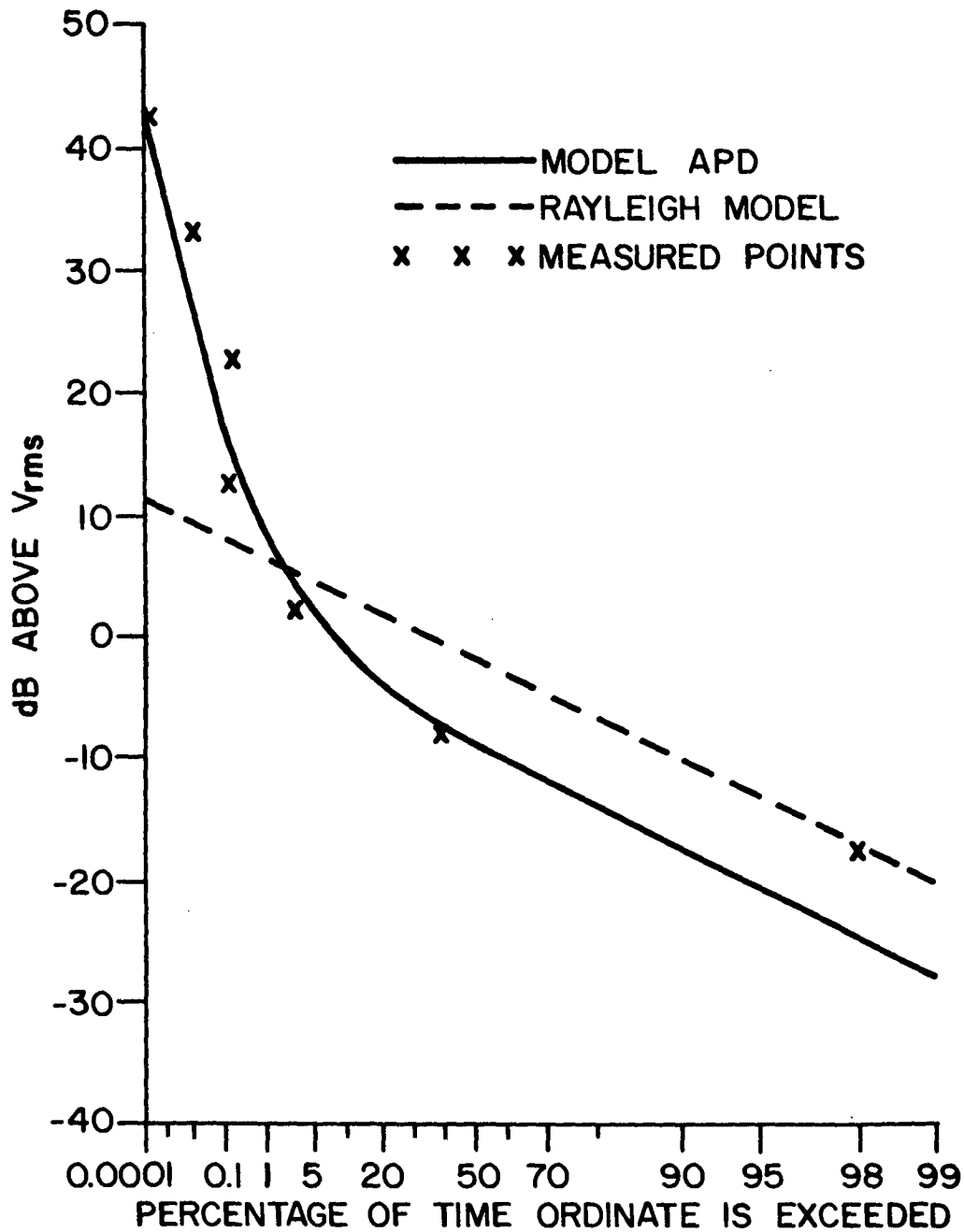

Figure 11. Typical APD Measure of Fit Found in Literature

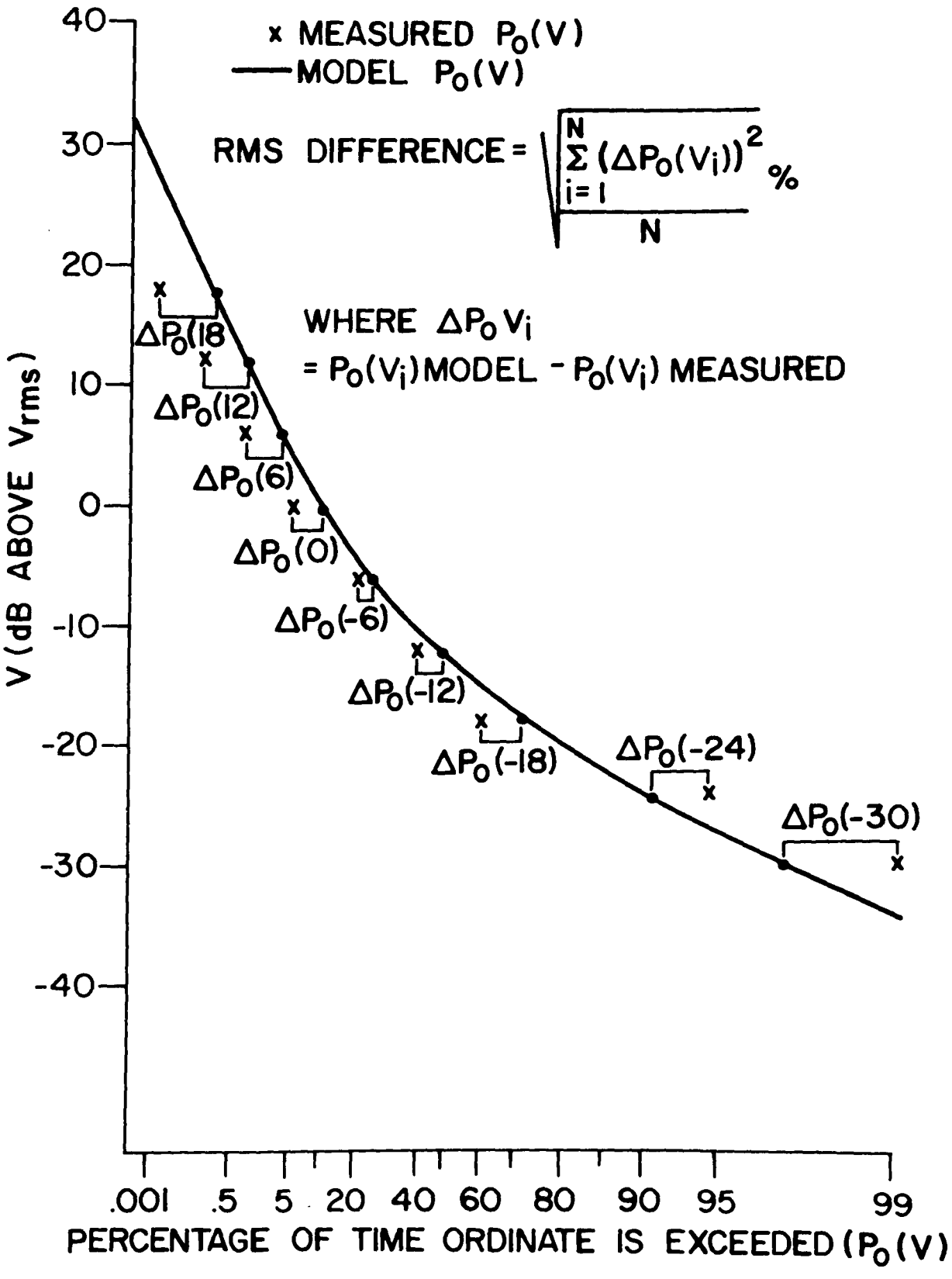

Figure 12. APD Measure of Fit for Models

Ideally one would use the measured values of V_{rms} and V_d as inputs to produce the model APDs, however, in this report, the calculated values of V_{rms} and V_d will be used for the model fits. This is necessary in order that the "errors" observed in the model tests may be accounted for in the models. As shown above (Section 3.3) there were differences on the order of ±2 dB between the calculated and measured values of V_{rms} and V_d. These differences have a significant effect on the model fits as shown in Figure 13 which is a cumulative distribution of the RMS Differences between the measured APDs and the Log-Normal model for the 125 distributions. The two lines show the results of using the measured values of V_{rms} and V_d and the calculated values of V_{rms} and V_d as inputs to the Log-Normal model. Similar curves were produced for the other three models. As an explanation of this figure, the perfect model would have a horizontal cumulative distribution at 0% RMS DIFFERENCE. Thus, the lower curve shows the better fit. The difference between the two curves is directly related to the difference between the measured and calculated values of V_{rms} and V_d. After the models have been adequately assessed, then one could use measured values of V_{rms} and V_d to predict accurately the APDs and ACRs and thus, the communication system performance.

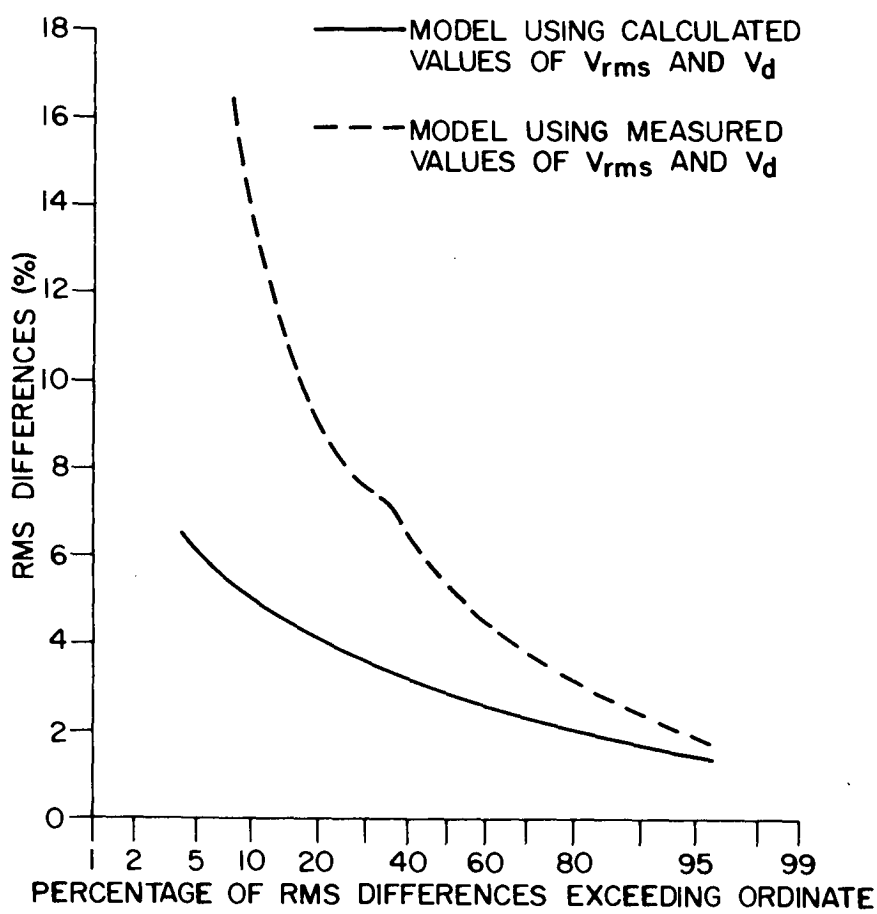

Figure 13. Cumulative Distribution of RMS DIFFERENCES Between the APD Measurements and the Log-Normal Model

Figure 14 shows the cumulative distributions of the RMS DIFFERENCES for the four models. The model APDs were produced with the calculated value of V_{rms} and V_d for each of the 125 distributions. As stated above, from the level and slope of the cumulative distribution, it is possible to select the "best" model for these data.

From the figure one can see that the Rayleigh model has an almost vertical line with a median RMS difference of 12.4%. This result could be inferred from the V_d measurements alone since Gaussian noise with a Rayleigh distributed envelope has a V_d of 1.05 dB and most of the measured values were between 2 and 6 dB. It can be used, however, as a reference to compare the performance of the other models. The RMS DIFFERENCES for the Rayleigh model were found to correlate well (r = 0.94) with the corresponding V_d values i.e., the higher the V_d value the larger the RMS DIFFERENCE between the measured APD and the Rayleigh model. The Log-Normal model seems to give the best fit with a mdeian RMS DIFFERENCE of 3% and a shallow slope. The Atmospheric model has the same median RMS DIFFERENCE of 5% as the Hall (θ=3) model but the Hall (θ=3) model has a steeper slope; i.e., a less consistent fit as shown by the larger variation. These model fits are much better than was found in the previous small sample discussed in Ref. 2 (a median RMS DIFFERENCE of 9% for the Atmospheric model and a median RMS DIFFERENCE of 6.5% for the Log-Normal model).

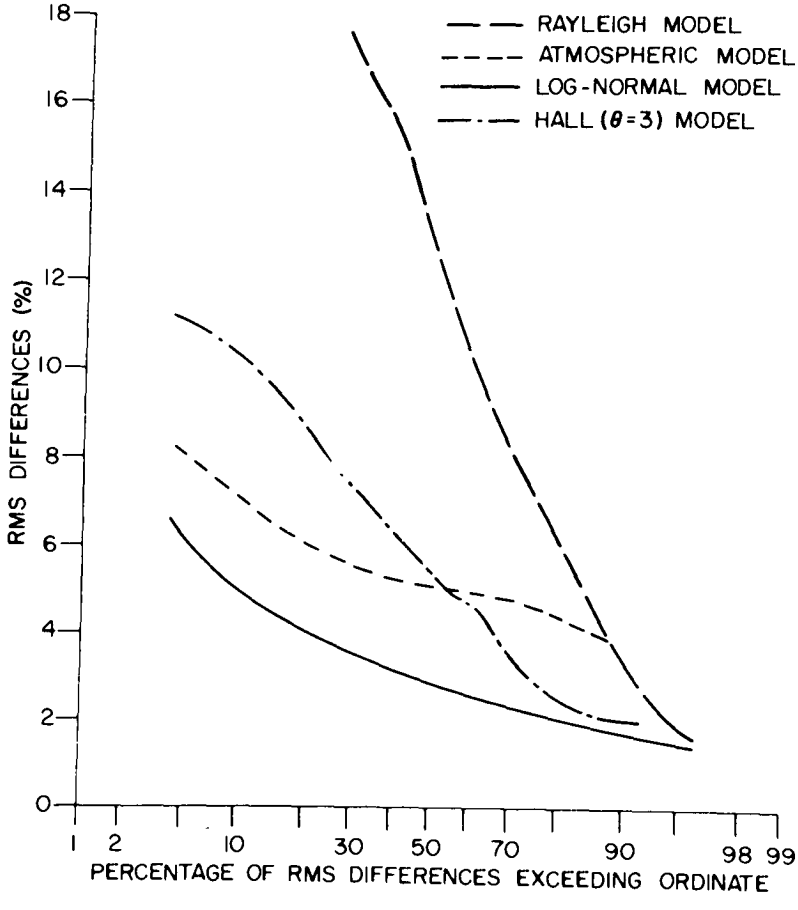

Figure 14. Cumulative Distribution of RMS DIFFERENCES Between the APD Measurements and the Four Models

Since the value of V_d is directly related to the shape of the APD, it was decided to vary it for the latter three models to optimize the fit, i.e., minimize the RMS DIFFERENCE. Figure 15 shows the results of minimizing the RMS DIFFERENCE of the three models on the 125 distributions. It shows the cumulative distribution of the RMS DIFFERENCE between the measured APDs and the models in a manner similar to that of Figure 14. Comparing Figures 14 and 15 one can see that the shapes of the curves are the same for the Log-Normal and Atmospheric models but that the levels are slightly lower, i.e., the median for the Log-Normal is 2.5% and the median for the Atmospheric model is 3.5% compared to 3% and 5% respectively. This shows that models were nearly best fits before the optimization. The greatest shape change occurred for the Hall (θ=3) model. It is now very nearly as good as the atmospheric noise model. However, one should look at the "cost" of the optimizing. For the 125 distributions, it was possible to produce the cumulative distributions of the change in the value of V_d (i.e., ΔV_d) necessary to produce the minimum RMS DIFFERENCE for each of the 125 distributions as shown in Figure 16. For the Log-Normal model, the changes were made under +0.5 dB at the deciles. The atmospheric model usually required an increase in V_d but again the change was less than 1 dB at the deciles. Both of these changes in V_d were well within the accuracy of the measurement and computation that produced the V_d values. The Hall (θ=3) model required the largest change in V_d to give the minimum RMS DIFFERENCE. 80% of the distributions required a decrease in V_d and the value of V_d was greater than 2 dB for as many as 30% of the distributions.

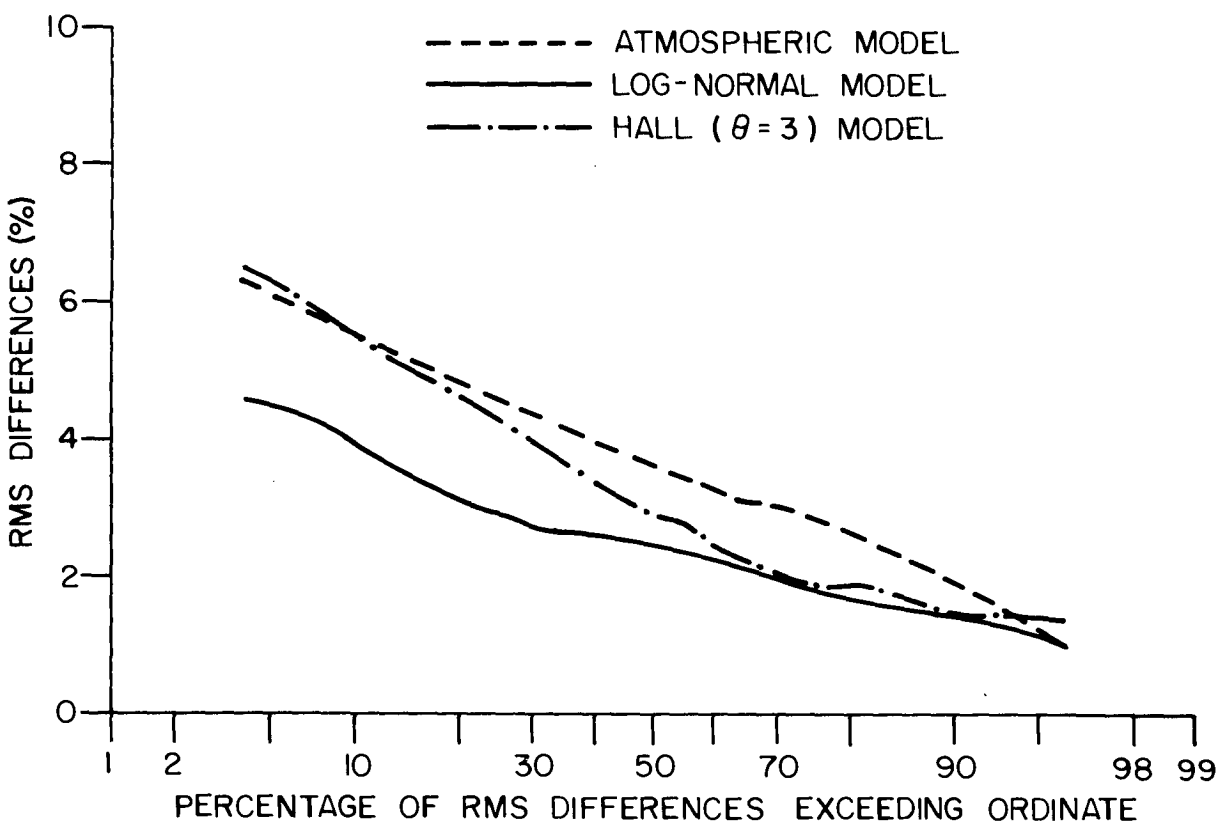

Figure 15. Cumulative Distribution of RMS DIFFERENCES Between the APD Measurements and the Three Models

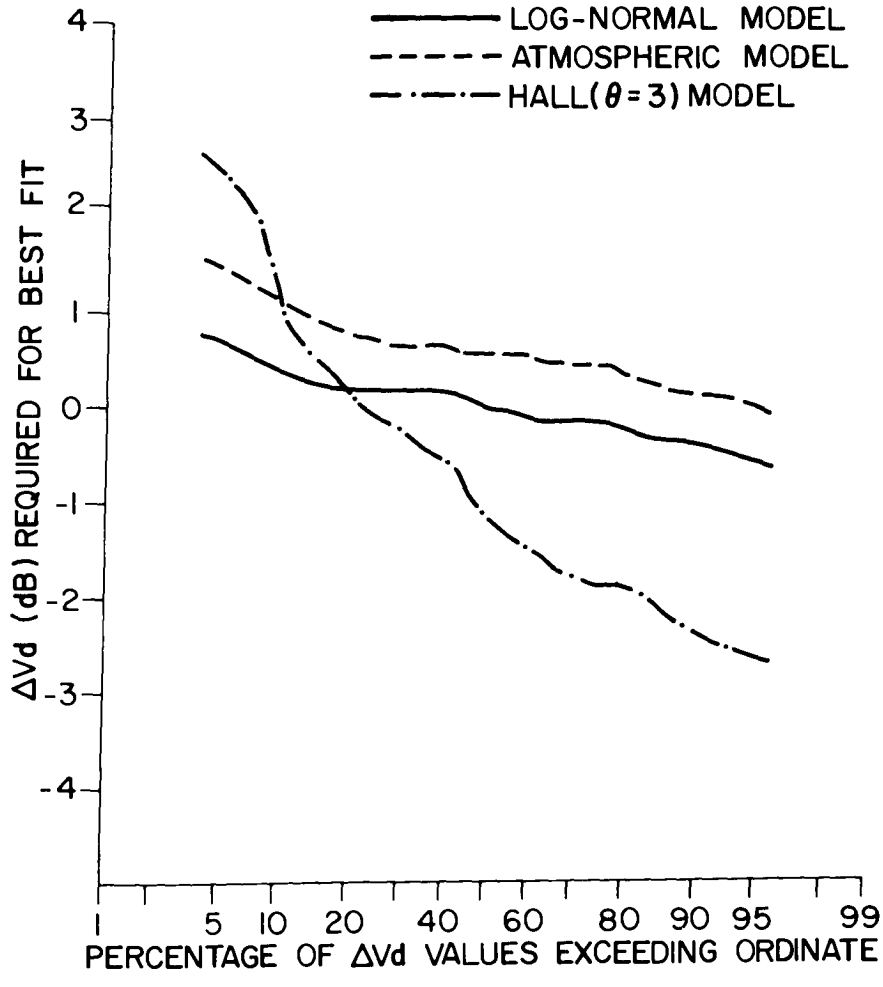

Figure 16. Cumulative Distribution of ΔV_d Values to Give Best Fit for Each Model

3.5 ACR DATA

Since all the temporal information about a noise process is lost during an APD measurement, a large number of different time waveforms could produce the same APD. This fact makes the temporal statistical distributions very important. It has been shown that the noise processes discussed in this report are not Gaussian. Of the three remaining models, mathematical expressions have been developed for the Average Crossing Rate (ACR) characteristic from the Log-Normal and Hall (θ=3) models.

These expressions output average crossing rates, $N^+(V)$ for a threshold, V. As with the APD's, there is a problem defining a measure of fit for the ACR measurement data and the two model expressions. A typical ACR characteristic has a very large range of values (as shown in Figure 17) and is very steep' i.e., for a variation of ±1 dB there is a large variation in function values. This is important when one remembers that the threshold of the RNA are set 6 dB apart with a possible error of ±1 dB.

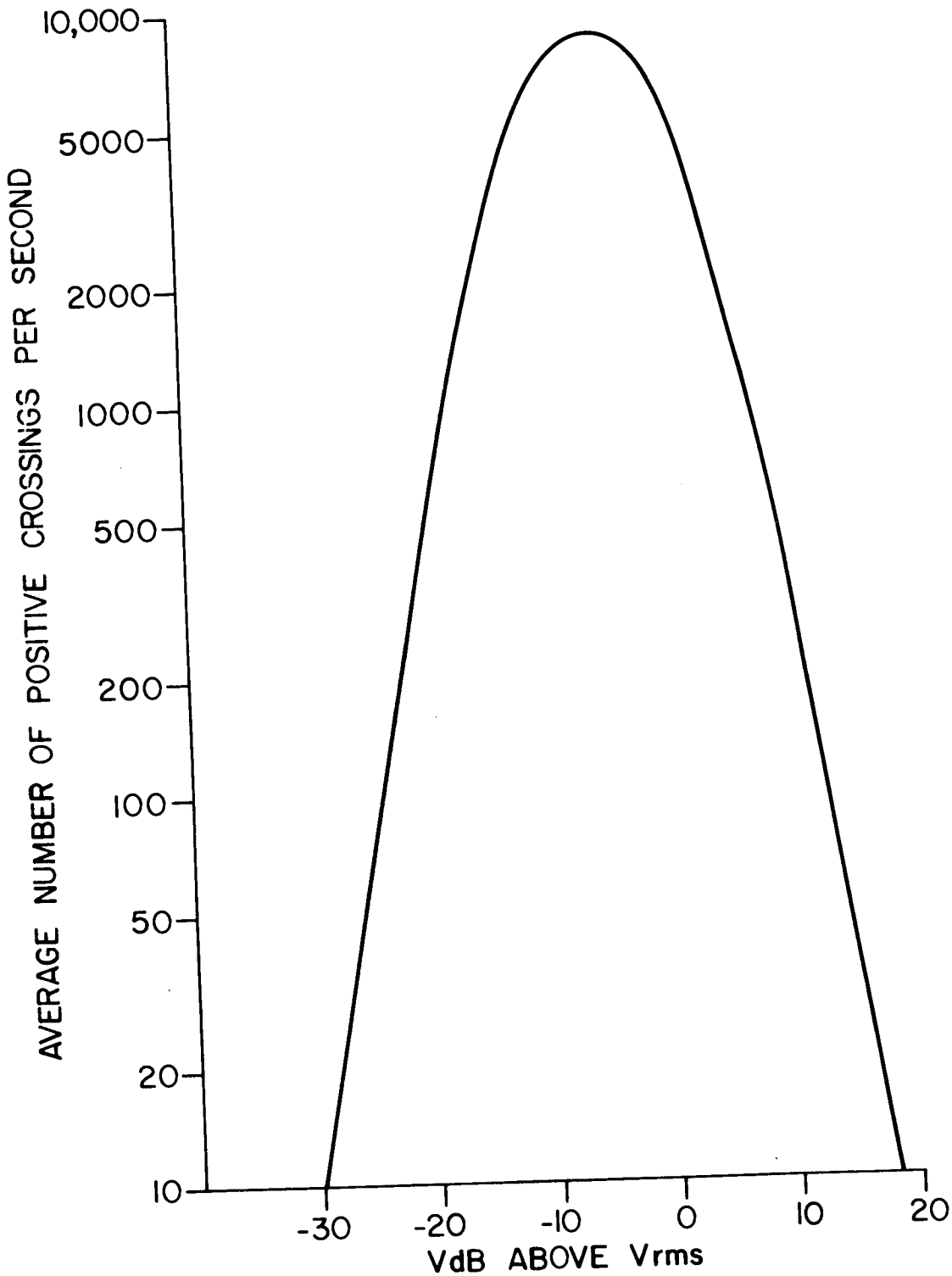

Figure 17. Typical ACR Characteristic

Also, for a goodness of fit test, it would be meaningless to do an RMS fit of ACR function values, i.e., a relatively small error to the top would far out-weigh a large discrepancy in the lower portion of the curve. Thus, it was decided to invert the models and for the measured values of $N^+(V)$ solve for a set of threshold, V_i. The measure of fit becomes the RMS DIFFERENCE of the levels as given by the following expression:

$$\text{RMS DIFFERENCE} = \sqrt{\frac{\sum_{i=1}^{N} (V_{i\ \text{model}} - V_{i\ \text{measured}})^2}{N}} \quad \text{(dB)} \tag{25}$$

This is illustrated in Figure 18 which shows some typical measured ACR data and a model curve. The RMS DIFFERENCE is computed for the levels and seems to be unbiased as to what part of the curve it is operating on.

The expression developed by Omura [14] for the ACR at a threshold V is:

$$N^+(V) = \frac{|\bar{\dot{N}}|}{2\pi\sigma_n^2}\, e^{\left| \frac{-(\ln (V/C))^2}{2\sigma_n^2} \right|} \tag{26}$$

where

$$\sigma_n^2 = \frac{V_d}{10 \log e}$$

$$C = \frac{V_{rms}}{e^{\sigma_n^2}}$$

as in equations 18 and 19. $|\bar{\dot{N}}|$ is the absolute value of the average of the derivative of the Gaussian noise process and depends on higher order statistics. This introduces a new parameter into the model and it is one that cannot be related directly to standard measurements. However, it is only a scaling factor, i.e., it moves the whole distribution up and down.

The expression for the ACR developed by Hall [15] at a threshold V is

$$N^+(V) = \frac{1}{2} \frac{\Gamma\left(\frac{\theta+2}{2}\right)}{\Gamma\left(\frac{\theta-1}{2}\right)} 8\pi^{\frac{1}{2}}\gamma^{\theta-1} B_c \frac{V}{(V^2+\gamma^2)^{\theta/2}} \tag{27}$$

This is a complicated expression to invert. However, for "large" threshold values it simplifies to:

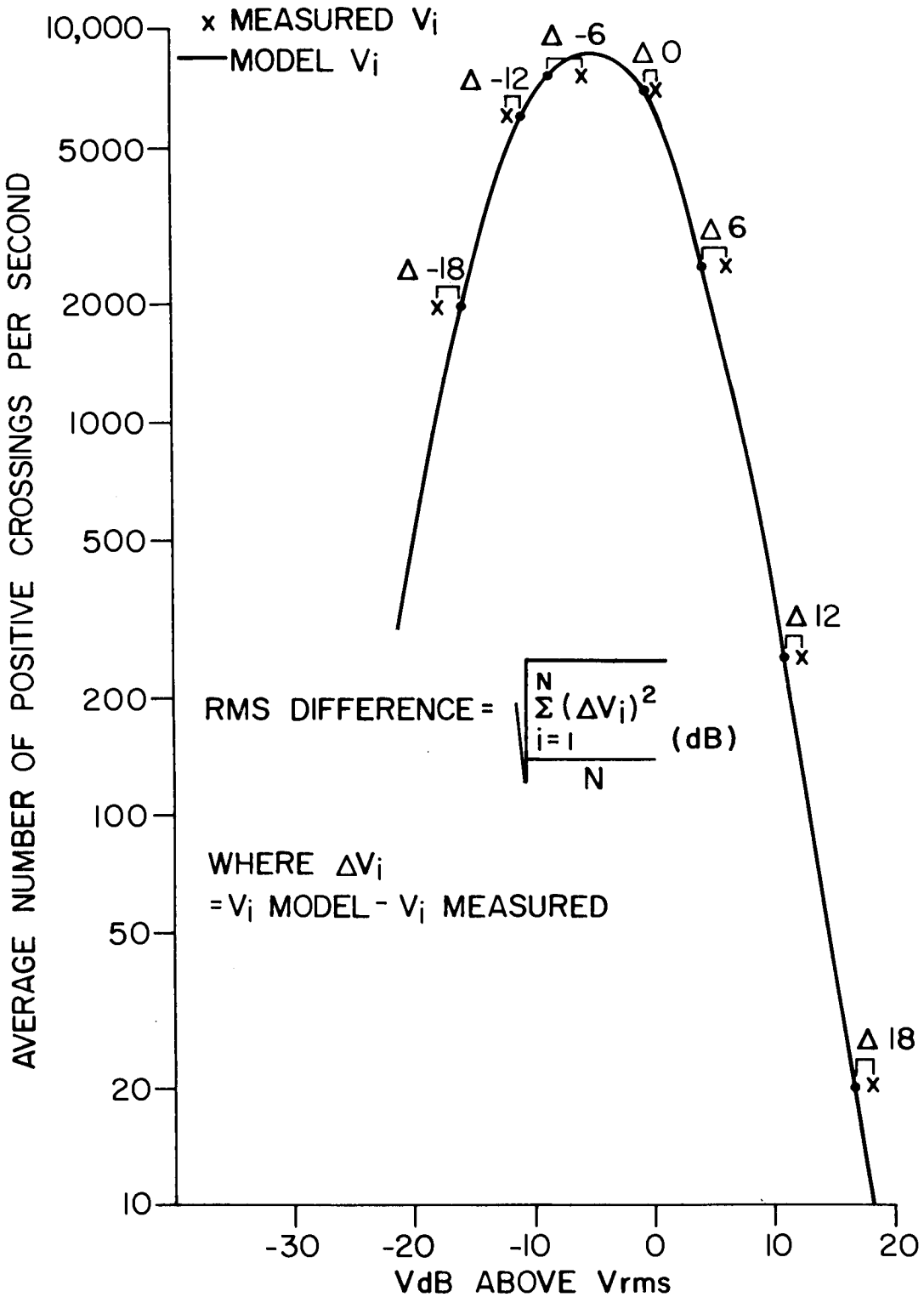

Figure 18. ACR Measure of Fit for Models

$$N^{+}(V) = \frac{8\pi^{\frac{1}{2}}}{2} \frac{\Gamma\left(\frac{\theta+2}{2}\right)}{\Gamma\left(\frac{\theta-1}{2}\right)} \frac{B_c}{\theta} \left(\frac{\gamma}{V}\right)^{\theta-1} \tag{28}$$

where B_c is the RMS bandwidth of the zero mean Gaussian process n(t)

$\theta = 3$

$\gamma = 2/\pi v_{average}$ as in equation 22.

As with the Log-Normal model, there again is a new parameter (scaling factor), B_c. For these tests, "large" was defined to be all thresholds to the right of the peak of the ACR characteristic. As above, this model was solved for a set of V_i's for each measured $N^{+}(V)$.

For a proper comparison of the two models we applied the Log-Noraml model only to values above the peak of the characterisitc, i.e., for the large values of the Hall model. For the Log-Normal model the value of $|\dot{N}|$ was varied to give the best fit, i.e., minimum RMS DIFFERENCE. It was possible to produce the cumulative distributions of the RMS DIFFERENCES between the measured characteristics and the models for the 125 characteristics (see Figure 19 for the Log-Normal model). Note that the curve has a shallow slope, indicating a consistent fit, and a median RMS DIFFERENCE of 4 dB. The values of $|\dot{N}|$ were found to vary between 7000 to 21,000 (between the deciles) with a median of 13,500; a variation of less than ±3 dB about the median. We next ran the model with $|\dot{N}|$ fixed at 13,500. The results of this are shown on the top line of Figure 19. This has the same shape as before, i.e., the model was just as consistent but shifted about 1 dB higher. This means that the RMS DIFFERENCE for each characteristic was increased by approximately 1 dB.

Figure 20 shows the cumulative distribution of the RMS DIFFERENCES between the measured ACRs and the Hall (θ=3) model. Here the value of B_c was varied to give the minimum RMS DIFFERENCE. The curve is very similar to Figure 19 and has a median value of 4.2 dB. The values of B_c have a median of 3200 Hz and a variation of ±2.5 dB about this median. When the model was run with a fixed value of B_c equal to 3200 Hz the top curve of Figure 20 resulted. Again the slope was the same, but the RMS DIFFERENCE from each characteristic was increased by approximately 0.5 dB. Both the Log-Normal and Hall (θ=3) models are about equal at predicting the ACR characteristic.

A word of caution is in order at this point. The values of $|\dot{N}|$ = 13,500 and B_c = 3200 Hz are only true for these tests and may vary considerably if another source of noise were used. The models, however, have been found to be relatively insensitive to these linear scaling parameters.

Since the measurement thresholds were set up with a possible error of only ±1 dB, the 4 dB RMS DIFFERENCES observed cannot be explained experimentally but must be due to limitations of the models. The major source of the noise, the powerline converter valves, added a dominant periodic component to the random noise process which the models could not account for. Figure 21 shows an example of the noise process. The valve firing is periodic but the

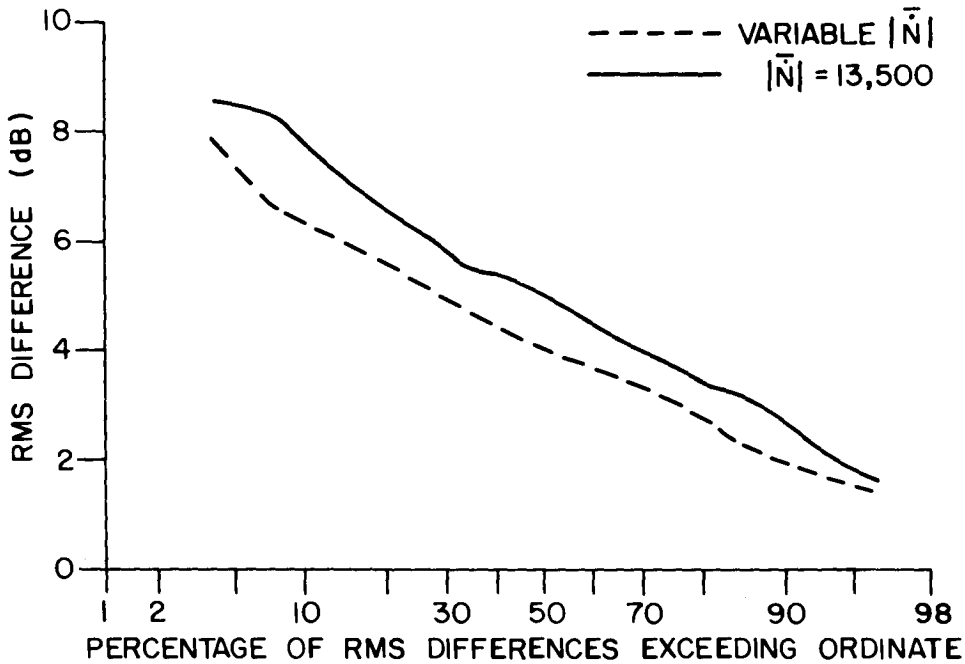

Figure 19. Cumulative Distributions of RMS DIFFERENCES Between the ACR Measurements and the Log-Normal Model

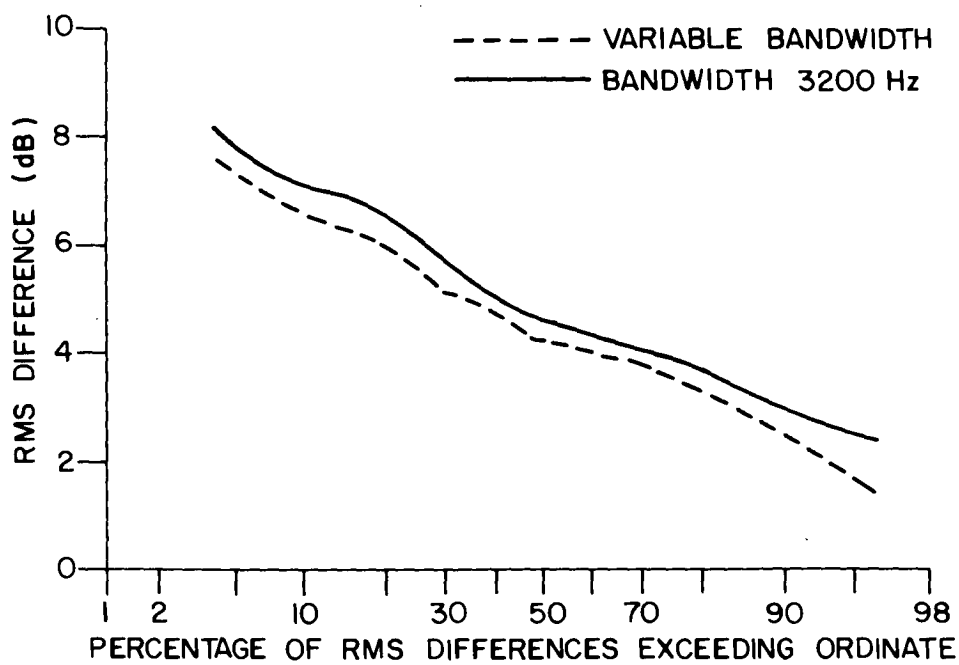

Figure 20. Cumulative Distributions of the RMS DIFFERENCES Between the ACR Measurements and the Hall (θ = 3) Model

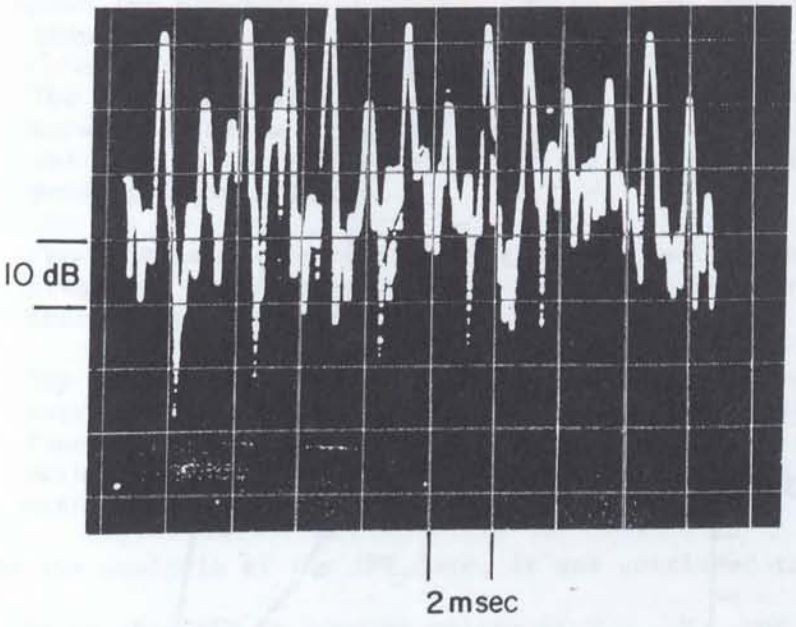

Figure 21. Temporal Display of HVDC Converter Station Radio Noise

amplitude are quite variable; on the order of 10 to 20 dB. If the valve firing pulses were of constant amplitude one would expect a "step" in the ACR characteristic at the valve firing rate. Since the amplitudes were not constant, the "step" (see Figure 22 for a typical measured ACR) is "sliding" and it is impossible to determine the actual firing rate of the valves from this characteristic. Also shown on Figure 22 is a line showing the Log-Normal model fit for this ACR. The model averages out the characteristic "step". This shows that these models cannot account for a periodic component which is very probable in most man-made noise processes, such as ignition noise.

4. SUMMARY AND CONCLUSIONS

Measurements of the HF (1 to 10 MHz) radio noise environment near an HVDC powerline converter station have been made under various line operating conditions. The measured noise was divided into three basic types: (i) converter valve noise; (ii) valve noise plus AC hum and (iii) valve noise plus DC corona. The DC corona was only observed at DC line voltages of ±450 KV.

1. From the analysis of the basic measurements, the following conclusions were arrived at:

   A. The measured average noise power levels were well above the CCIR predicted levels for a rural area and the DC corona levels were above the CCIR business line.

   B. The average noise power levels were found to decrease with increasing frequency at a rate of twice that predicted by

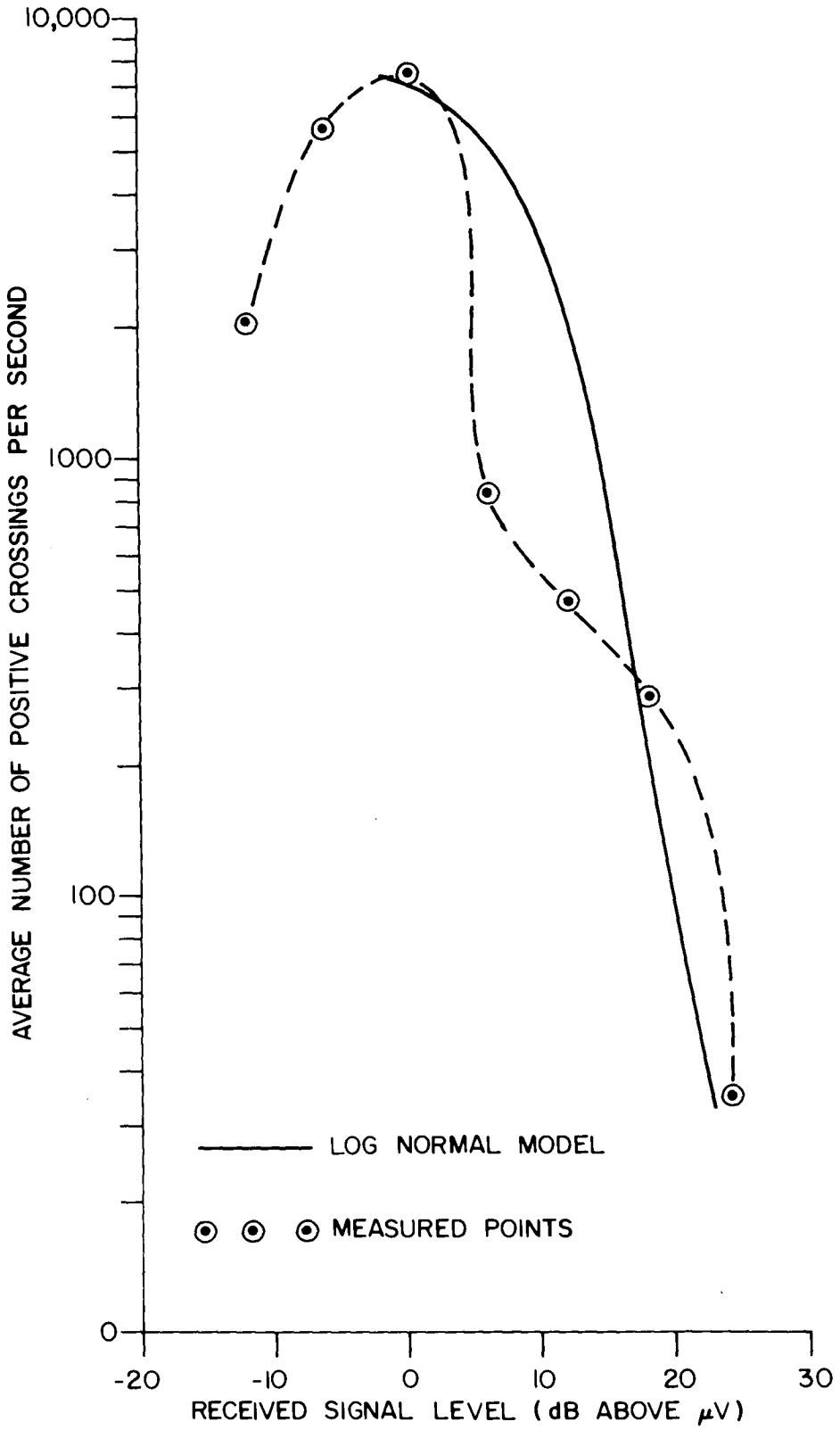

Figure 22. Typical Average Crossing Rate Characteristic of HVDC Converter Station Radio Noise

CCIR for man-made noise, i.e., 50 to 60 dB per decade rather than 27.7 dB.

C. The V_d values which characterize the impulsiveness of the noise were at or below the rural predictions except for the converter valve noise where they were found to be significantly above the predicted rural values.

D. The V_d values were relatively constant as a function of frequency with a one to two dB per decade decrease with increasing frequency.

E. The quasi peak levels follow the same general trend as the average power levels of the highest to lowest values as a function of location and type of noise; however, the variation with frequency was less (-30 to -40 dB per decade as compared with -50 to -60).

2. From the analysis of the APD data, it was concluded that:

A. It is possible to compute values of V_{rms}, V_d, and V_{qp} from the APD data that are accurate to within the accuracy of present day measuring equipment.

B. For these types of noise the value of Q_d (20 log V_{qp}/V_{rms}) was found to be 12 dB ±2 dB. The small value of the standard deviation was of the same order as the accuracy of most meters used for making these measurements.

3. The Rayleigh model and three other mathematical models originally developed to characterize atmospheric noise have been fitted to the measured APD data. The RMS DIFFERENCE between the model and measured APD's (probabilities) was used as the measure of fit with which to compare the performance of the four models. From this analysis, it was shown that:

A. These measurements were from impulsive rather than Gaussian noise.

B. The Log-Normal model produced APD's that compared more closely to the measured ones.

4. Expressions from the Log-Normal and Hall models were used to fit the measured ACR data. The original model expressions for the ACR characteristics were inverted to give a measure of fit of the RMS DIFFERENCE between the model and measured threshold levels. It was concluded that:

A. Both the Log-Normal and the Hall model expressions fit the measured ACR data equally well.

B. The periodic component of the noise, introduced by the converter valves did not affect the APD models but was very evident in the ACR data and was not accounted for in the ACR expressions of the random noise models.

5. REFERENCES

1. IEEE Committee, *A Field Comparison of RI and TVI Instrumentation*, IEEE Transactions on Power Apparatus and Systems, Vol. PAS-96, No. 3, May/June 1977, pp. 863-875.

2. Lauber, W.R., *Amplitude Probability Distribution Measurements at the Apple Grove 775 kV Project*, IEEE Transactions on Power Apparatus and Systems, Vol. PAS-95, No. 4, July/August, 1976, pp. 1254-1266.

3. Morse, A.R., I.G. Jeffrey and M. Bulawka, *Field Measurements on the Nelson River HVDC Line*, Proceedings of the Canadian Communications and Power Conference, Montreal, Quebec, IEEE Catalogue No. 76CH1126-2REG-7, October 1976.

4. Morse, A.R., *Field Measurements of Station-Generated RI on the Nelson River HVDC Line in 1976*, Conference Digest, International Electrical, Electronics Conference and Exposition, Toronto, Ontario, IEEE Catalogue No. 77CH1256-7REG-7, September 1977.

5. Morris, R.M., A.R. Morse, J.P. Griffin, O.C. Norris Elye, C.V. Thio and J.S. Goodman, *The Corona and Radio Interference Performance of the Nelson River HVDC Transmission Lines*, Paper No. F79 236-1 presented at the IEEE Power Engineering Society's Winter Power Meeting, New York, February 1979.

6. Middleton, D., *Introduction to Statistical Communication Theory*, McGraw Hill, New York, 1960.

7. URSI, *The Measurement of Characteristics of Terrestrial Radio Noise*, Special Report No. 7, International Union of Radio Science, Elseviar Publishing Co., Amsterdam, 1962.

8. Bendat, J.S. and A.G. Piersol, *Random Data: Analysis and Measurement Procedures*, Wiley-Interscience, New York, 1971.

9. CCIR, *World Distribution and Characteristics of Atmospheric Radio Noise*, Report 322, International Radio Consultative Committee, Geneva, Switzerland, 1963.

10. Burrill, C.M., *An Evaluation of Radio Noise Meter Performance in Terms of Listening Experience*, Proceedings of IRE, Vol. 30, No. 10, October 1942, pp. 473-478.

11. Montgomery, G.F., *A Comparison of Amplitude and Angle Modulation for Narrow-Band Communication of Binary-Coded Messages in Fluctuation Noise*, Proceedings of IRE, Vol. 42, February 1954, pp. 447-454.

12. Bello, P.A., *Error Probabilities Due to Atmospheric Noise and Flat Fading in HF Ionospheric Communication Systems*, IEEE Transactions on Communication Technology, Vol. 13, No. 3, September 1965, pp. 266-279.

13. Akima, H., G.G. Ax, W.M. Berry, *Required Signal-to-Noise Ratios for HF Communication Systems*, ESSA Technical Report ERL 131-ITS 92, Boulder, Colorado, August 1969.

14. Omura, J.K., *Statistical Analysis of LF/VLF Communications Modems*, Special Technical Report 1 SRI Project 7045, Stanford Research Institute, Menlo Park, California, August, 1969.

15. Hall, H.M., *A New Model for 'Impulsive' Phenomena: Application to Atmospheric Noise Communication Channels*, Stanford University Electronics Laboratories Technical Report No. 7050-7, Stanford, California, August 1966.

16. Giordano, A.A. and F. Haber, *Modelling of Atmospheric Noise*, Radio Science, Vol. 7, No. 11, November 1972, pp. 1011-1023.

17. Blake, I.F. and W.C. Lindsey, *Level-Crossing Problems for Random Processes*, IEEE Transactions on Information Theory, Vol. IT-19, No. 3, May 1973, pp. 295-315.

18. Lauber, W.R. and J.M. Bertrand, *A Radio Noise Analyzer*, CRC Technical Note 696, Ottawa, Ontario, January 1979.

19. Matheson, R.J., *Instrumentation Problems Encountered Making Man-Made Electromagnetic Noise Measurements for Predicting Communication System Performance*, IEEE Transactions on Electromagnetic Compatibility, Vol. EMC-12, No. 4, November 1970, pp. 151-158.

20. *Proceedings of the National Power Conference EHV-DC*, Edited by M.Z. Tarnaweky, Winnipeg, Manitoba, June 1971.

21. CCIR, *Man-Made Radio Noise*, Report 258-3, International Radio Consultative Committee, Geneva, Switzerland, 1978.

22. Spaulding, A.D. and R.T. Disney, *Man-Made Radio Noise Part 1: Estimates for Business, Residential and Rural Areas*, U.S. Department of Commerce OT Report 74-38, Boulder, Colorado, June 1974.

23. Cook, J.H., *Quasi-Peak-to-RMS Voltage Conversion*, IEEE Transactions on Electromagnetic Compatibility, Vol. EMC-21, No. 1, February 1979, pp. 9-12.

24. Spaulding, A.D., *Man-Made Noise: The Problem and Recommended Steps Toward Solution*, OT Report 76-85, Office of Telecommunications, U.S. Department of Commerce, Boulder, Colorado, April 1976.

25. Middleton, D., *Statistical-Physical Models of Man-Made Radio Noise, Part I: First-Order Probability Models of the Instantaneous Amplitude*, Office of Telecommunications Report 74-36, Boulder, Colorado, April 1974.

26. Middleton, D., *Statistical-Physical Models of Man-Made and Natural Radio Noise, Part II: First-Order Probability Models of the Envelope and Phase*, Office of Telecommunications Report 76-86, Boulder, Colorado, April 1976.

27. Middleton, D., *Statistical-Physical Models of Man-Made and Natural Radio Noise, Part III: First-Order Probability Models of the Instantaneous Amplitude of Class B Interference,* National Telecommunications and Information Administration Report NTI-CR-78-1, Boulder, Colorado, June 1978.

28. Middleton, D., *Statistical-Physical Models of Man-Made and Natural Radio Noise, Part IV: Determination of the First-Order Parameters of Class A and B Interference,* National Telecommunications and Information Administration, Report NTLA-CR-78-2, Boulder, Colorado, September 1978.

29. Spaulding A.D. and D. Middleton, *Optimum Reception in an Impulsive Interference Environment,* Office of Telecommunications Report 75-67, Boulder, Colorado, June 1975.

30. Landon, V.D., *The Distribution of Amplitude With Time in Fluctuation Noise,* Proc. IRE, Vol. 29, February 1941, pp. 50-55. See also K.A. Norton, *Discussion on the Distribution of Amplitude With Time in Fluctuation Noise,* Proc. IRE, Vol. 30, September 1942, pp. 425-429.

31. Crichlow, W.Q., C.J. Roubique, A.D. Spaulding and W.A. Berry, *Determination of the Amplitude Probability Distribution of Atmospheric Radio Noise from Statistical Measurements,* Journal of Research of the National Bureau of Standards, Vol. 64D, No. 1, January to February 1960, pp. 40-56.

32. Spaulding, A.D., C.J. Roubique and W.Q. Crichlow, *Conversion of the Amplitude Probability Distribution Function for Atmospheric Radio Noise from One Bandwidth to Another,* Journal of Research of the National Bureau of Standards, Vol. 66D, No. 6, November to December 1962, pp. 713-720.

33. Akima, H., *A Method of Numerical Representation for the Amplitude Probability Distribution of Atmospheric Radio Noise,* Office of Telecommunications Research and Engineering Report OT/TRER 27, Boulder, Colorado, March 1972.

34. Beckmann, P., *Amplitude Probability Distribution of Atmospheric Radio Noise,* Radio Science, Vol. 68D, June 1964, pp. 723-736.

35. Schonoff, T.A., A.A. Giordano and Z. MacHuntoon, *Analytical Representations of Atmospheric Noise Distributions Constrained in V_d,* Conference on Communications, Vol. 1, Chicago, Illinois, IEEE Catalogue No. 77CH1209-6CSCB, June 1977.

36. Giordano, A.A., *Modelling of Atmospheric Noise,* Ph.D. Thesis, Graduate School of Arts and Sciences, University of Pennsylvania, Philadelphia, Pennsylvania, 1970.

37. Siegel, S., *Nonparametric Statistics for the Behavioural Sciences,* McGraw-Hill Book Company, New York, 1956.

APPENDIX A

F_a, V_d AND RI (V_{qp}) MEASURED DATA

Test No.	Frequency (MHz)	F_a (dB above kT)	V_d (dB)	RI (dB above 1 μv/m)
1 — July 23, 1977 at DC site 1 with DC line operating at ±150KV (550A)				
	1.1	93.7	5.2	49.6
	1.5	86.1	4.8	43.4
	2.0	80.7	5.5	42.7
	2.5	78.3	4.5	—
	3.0	72.9	5.2	—
	4.0	57.5	3.8	—
	5.0	53.7	2.8	—
	6.0	41.3	2.2	—
	7.0	37.8	1.8	—
	8.0	37.3	1.6	—
	9.0	37.2	2.0	—
	10.0	32.5	2.4	—
2 — July 23, 1977 at DC site 1 with DC line operating at $\begin{matrix}-450\\+300\end{matrix}$KV (700A)				
	1.1	95.2	3.0	49.1
	1.5	90.9	3.8	48.4
	2.0	88.2	4.8	50.7
	2.5	81.6	4.5	42.7
	3.0	73.2	4.0	37.5
	4.0	65.8	3.2	32.4
	5.0	60.2	3.0	26.2
	6.0	51.3	3.2	17.4
	7.0	44.6	1.2	10.0
	2.0	88.2	4.8	50.7
	2.5	81.6	4.0	42.7
	3.0	73.2	3.0	38.5
	5.0	59.3	2.5	28.2
3 — July 23, 1977 at DC site 2 with DC line operating at $\begin{matrix}-450\\+300\end{matrix}$KV (780A)				
	1.1	91.7	1.8	44.1
	1.5	82.4	1.8	35.9
	2.0	79.1	1.5	34.7
4 — July 24, 1977 at DC site 1 with DC line not operating				
	1.1	78.7	5.0	30.1
	2.0	66.2	2.0	24.7
	3.0	63.4	2.5	20.5
	4.0	57.3	2.2	13.9
	5.0	56.7	2.0	18.2
	6.0	52.3	4.0	6.4
	7.0	52.6	4.0	3.0
	8.0	45.1	2.0	2.7
	9.0	45.7	3.0	1.3
	10.0	38.0	2.0	2.5

Test No.	Frequency (MHz)	F_a (dB above kT)	V_d (dB)	RI (dB above 1 μv/m)
5 — July 24, 1977 at AC site 1 with DC line operating at ±300KV (500A)				
	1.1	95.2	2.0	46.1
	1.5	92.1	2.8	48.4
	2.0	86.2	4.0	46.7
	2.5	80.8	3.2	39.2
	3.0	72.4	2.2	32.5
	4.0	66.8	2.0	27.9
	5.0	61.9	1.8	29.2
	6.0	51.8	1.8	19.4
	7.0	50.1	1.8	14.0
	8.0	47.6	2.6	16.7
	9.0	45.7	2.2	13.3
	10.0	40.5	1.8	9.5
6 — July 24, 1977 at AC site 2 with DC line operating at ±300KV (830A)				
	1.1	93.2	1.2	45.1
	1.5	83.4	2.2	42.9
	2.0	84.2	2.0	37.7
	2.5	77.0	2.2	37.2
	3.0	73.4	2.2	38.5
	4.0	65.3	1.8	25.9
	5.0	58.7	1.2	—
7 — July 25, 1977 at DC site 1 with DC line operating at ±300KV (1000A)				
	1.1	99.7	5.2	50.1
	1.5	89.9	4.2	44.9
	2.0	89.2	2.8	48.7
	2.5	80.8	3.8	41.2
	3.0	71.9	4.0	35.5
	4.0	64.6	3.0	28.9
	5.0	60.2	2.5	26.2
	6.0	51.3	2.8	17.4
	7.0	42.6	2.0	14.0
	8.0	45.1	4.0	16.7
	9.0	41.7	3.0	11.3
	10.0	39.0	3.5	11.5
8 — July 25, 1977 at DC site 1 with DC line operating at ±300KV (500A)				
	1.1	93.7	5.0	45.1
	1.5	89.4	5.2	46.9
	2.0	87.2	7.0	49.7
	2.5	80.3	5.5	41.2
	3.0	72.9	5.0	37.5
	4.0	64.1	2.8	28.9
	5.0	58.2	3.2	25.2
	6.0	47.8	3.5	15.4
	7.0	42.6	2.8	13.0
	8.0	43.6	4.0	15.7
	9.0	39.7	2.2	12.3
	10.0	39.0	3.8	14.5

Test No.	Frequency (MHz)	F_a (dB above kT)	V_d (dB0	RI (dB above 1 μv/m)
9 – July 25, 1977 at DC site 2 with DC line operating at ±300KV (1000A)				
	1.1	93.7	4.5	50.1
	1.5	83.4	3.0	39.9
	2.0	78.7	4.8	40.7
	2.5	77.0	3.8	39.2
	3.0	63.4	5.0	30.5
	4.0	56.3	2.0	16.9
	5.0	54.7	3.0	22.2
	6.0	43.3	2.0	11.4
	9.0	35.7	1.6	3.3
	10.0	36.0	1.0	6.5
10 – July 25, 1977 at DC site 3 with DC site 3 with DC line operating at ±300KV (1000A)				
	1.1	84.5	2.2	34.1
	1.5	76.9	3.0	37.9
	2.0	71.2	2.2	30.7
	2.5	64.8	1.0	24.2
	3.0	60.9	1.8	21.5
	4.0	55.8	2.0	17.9
	5.0	54.7	2.5	20.2
11 – July 25, 1977 at DC site 1 (15 m) with DC line operating at $\begin{matrix}-300\\+150\end{matrix}$KV (1320A)				
	1.5	87.4	3.0	42.9
	2.5	76.8	4.2	38.2
	5.0	55.7	3.5	26.2
12 – July 25, 1977 at DC site 1 (30 m) with DC line operating at $\begin{matrix}-300\\+150\end{matrix}$ KV (1320A)				
	1.5	81.9	3.8	38.9
	2.5	79.8	3.5	40.2
	5.0	56.7	1.5	25.2
13 – July 26, 1977 at Clarkleigh 1 with DC line operating at $\begin{matrix}-450\\+300\end{matrix}$KV (900A)				
	1.1	83.7	1.5	31.1
	1.5	88.7	3.0	37.9
	2.0	71.4	1.0	25.7
	2.5	66.3	1.0	25.2
	3.0	63.4	1.0	21.5
	4.0	56.3	1.0	16.9
	5.0	52.7	1.0	16.2

Test No.	Frequency (MHz)	F_a (dB above kT)	V_d (dB)	RI (dB above 1 μv/m)
14 – July 26, 1977 at Clarkleigh 2 with DC line operating at $\begin{matrix}-450\\+300\end{matrix}$KV (900A)				
	1.1	87.2	3.8	40.1
	1.5	74.9	1.5	29.9
	2.0	69.2	1.0	50.7
	2.5	66.3	1.0	42.2
15 – July 26, 1977 at AC site 3 with DC line operating at $\begin{matrix}-450\\+300\end{matrix}$KV (810A)				
	1.1	90.7	2.5	53.1
	1.5	89.4	2.2	44.9
	2.0	86.7	4.0	45.7
	2.5	86.3	4.5	48.2
	3.0	78.9	3.5	42.5
	4.0	69.8	2.5	33.9
	5.0	60.9	2.5	25.2
	6.0	61.3	3.2	31.4
	8.0	53.1	1.0	21.7
	10.0	49.0	1.2	19.5
16 – July 27, 1977 at DC Site 1 corner with DC line operating at ±150KV (400A)				
	1.5	88.9	1.4	32.9
	2.0	76.2	3.0	34.7
	2.5	69.8	3.2	29.2
	3.0	66.4	2.5	26.0
	4.0	58.8	2.5	21.9
	5.0	54.2	1.5	20.2
	6.0	48.8	2.0	11.4
	7.0	47.1	3.5	12.0
	8.0	44.6	1.5	9.7
	9.0	43.7	3.5	8.3
	10.0	39.5	1.8	8.5
17 – July 27, 1977 at DC Site 2 corner with DC line operating at ±150KV (400A)				
	1.1	79.5	3.2	35.1
	2.0	72.2	2.5	33.7
	4.0	61.3	1.5	20.4
	6.0	50.3	3.2	11.4
	8.0	42.6	2.5	6.7
	10.0	35.0	2.5	2.5

Test No.	Frequency (MHz)	F_a (dB above kT)	V_d (dB)	RI (dB above 1 μv/m)	Distance from Outside Conductor
18 – July 27, 1977 at Site 1 (15–30 m) with DC line operating at ±300KV (1140A)					
	1.5	87.4	5.0	45.9	15
	1.5	81.9	4.0	38.9	30
	2.0	84.7	4.0	46.7	30
	2.0	86.7	3.5	46.7	15
	2.5	79.3	5.0	39.2	15
	2.5	78.3	5.2	39.2	30
	4.0	62.3	4.0	27.9	30
	4.0	59.3	4.8	27.9	15
	5.0	57.7	3.0	26.2	15
	5.0	56.7	4.0	26.2	30
	8.0	45.1	4.8	14.7	30
	8.0	44.1	3.8	11.7	15
	10.0	39.5	3.0	12.5	15
	10.0	38.5	1.5	8.5	30
19 – July 27, 1977 at DC Ground Site 1 with DC line operating at $\begin{matrix}-450\\+300\end{matrix}$KV (920A)					
	1.5	85.4	4.5	42.9	
	2.0	86.2	5.5	45.7	
	2.5	81.3	5.0	43.2	
	4.0	69.8	4.8	36.9	
	5.0	62.2	4.5	30.2	
	8.0	40.6	1.5	7.7	
	10.0	39.5	1.5	12.5	
20 – July 27, 1977 at DC Ground Site 2 with DC line operating at $\begin{matrix}-450\\+300\end{matrix}$KV (920A)					
	1.5	89.4	5.5	44.9	
	2.0	85.2	5.0	43.7	
	2.5	84.8	5.2	46.2	
	4.0	69.3	2.5	31.9	
	5.0	67.7	4.5	35.2	
	8.0	44.6	2.8	14.7	
	10.0	44.0	2.5	11.5	
21 – July 28, 1977 at DC Site 1 with DC line operating at ±450Kv (800A)					
	1.1	100.7	1.6	50.1	
	1.5	95.4	2.8	48.9	
	2.0	93.7	2.2	53.7	
	2.5	89.0	3.6	48.2	
	3.0	77.4	1.8	37.5	
	4.0	72.3	2.0	35.9	
	5.0	71.5	1.8	36.2	
	6.0	63.8	1.0	29.4	
	10.0	55.0	1.5	24.5	

CRC DOCUMENT CONTROL DATA

1. **ORIGINATOR:** Department of Communications/Communications Research Centre

2. **DOCUMENT NO:** CRC Report No. 1362

3. **DOCUMENT DATE:** March 1983

4. **DOCUMENT TITLE:** Measurements and Modelling of the HF Radio Noise Environment Near an HVDC Converter Station

5. **AUTHOR(s):** W.R. Lauber and J.M. Bertrand

6. **KEYWORDS:**
(1) Measurements
(2) Powerline
(3) Noise

7. **SUBJECT CATEGORY (FIELD & GROUP: COSATI)**

17 Navigation, Communications, Detection, and Countermeasures

17 02 Communications

8. **ABSTRACT:**

Measurements of the HF radio noise environment near an HVDC transmission line and converter station were made outside Winnipeg in July 1977. Typical levels and characteristics are presented for various combinations of mercury arc valve noise, AC hum and DC corona from a number of sites within eight kilometres of the converter station. In addition, two sets of measurements were taken 80 km from the converter station. Values of the root-mean-square, average and quasipeak voltages were calculated from the Amplitude Probability Distribution (APDs) of the noise and were found to compare favourably with the directly measured values. Four mathematical models, the Rayleigh and three others which were developed for atmospheric noise were fitted to the measured APD data. Using inputs of V_{rms} and V_d the Log-Normal model produced the most accurate predictions of the measured APDs. The Log-Normal and the Hall models both fitted the measured Average Crossing Rate data equally well.

9. **CITATION:**

Government of Canada Gouvernement du Canada